NANO · MICRO small
www.small-journal.com

On-Demand Removable Self-Healing and pH-Responsive Europium-Releasing Adhesive Dressing Enables Inflammatory Microenvironment Modulation and Angiogenesis for Diabetic Wound Healing

Meimei Fu, Yitao Zhao, Yue Wang, Yue Li, Min Wu, Qi Liu, Zhiguo Hou, Zhihui Lu, Keke Wu, and Jinshan Guo**

Current diabetic wound treatments remain unsatisfactory due to the lack of a comprehensive strategy that can integrate strong applicability (tissue adhesiveness, shape adaptability, fast self-healability, and facile dressing change) with the initiation and smooth connection of the cascade wound healing processes. Herein, benefiting from the multifaceted bonding ability of tannic acid to metal ions and various polymers, a family of tannin–europium coordination complex crosslinked citrate-based mussel-inspired bioadhesives (TE-CMBAs) are specially developed for diabetic wound healing. TE-CMBAs can gel instantly (< 60 s), possess favorable shape-adaptability, considerable mechanical strengths, high elasticity, considerable wet tissue adhesiveness (≈40 kPa), favorable photothermal antimicrobial activity, excellent anti-oxidant activity, biocompatibility, and angiogenetic property. The reversible hydrogen bond crosslinking and sensitive metal–phenolic coordination also confers TE-CMBAs with self-healability, pH-responsive europium ion and TA releasing properties and on-demand removability upon mixing with borax solution, enabling convenient painless dressing change and the smooth connection of inflammatory microenvironment modulation, angiogenesis promotion, and effective extracellular matrix production leveraging the acidic pH condition of diabetic wounds. This adhesive dressing provides a comprehensive regenerative strategy for diabetic wound management and can be extended to other complicated tissue healing scenarios.

1. Introduction

Diabetes affects over 536 million people, and its prevalence will further increase to 783 million by 2045 with the rapidly aging population worldwide.[1] Around 25% of diabetics face a lifetime risk of chronic nonhealing wounds represented as diabetic foot ulcers (DFUs), which causes enormous pain, and often lead to amputation with a high mortality ratio (at least 68% die in five years).[2–5] Acute wounds normally heal in several weeks after finishing three highly organized and overlapping phases: inflammation, proliferation, and remodeling.[2,3,6] However, diabetic chronic wounds are often stuck in a persistent inflammatory state, characterized by elevated levels of reactive oxygen species (ROS) and pro-inflammatory cytokines, angiogenesis disorders, imbalance of matrix metalloproteinases and their inhibitors, as well as bacterial infection and colonization, thus are difficult to heal.[3,7–10] Extensive efforts have been devoted to addressing this challenge. Except for the control of blood glucose and surgical debridement, the addition of antibiotics, anti-inflammatory drugs, platelet-rich plasma (PRP), exosomes, and growth factors into wound dressings were also used in the treatment of diabetic wounds,[11–14] but drug resistance, side effects, inaccessibility, and instability of these bioactive agents cannot be ignored. Recently, extensive regenerative medicine endeavors aimed to promote angiogenesis,[13,15,16] control bacterial infection,[15,17]

M. Fu, Y. Zhao, Y. Wang, Y. Li, M. Wu, Z. Lu, K. Wu, J. Guo
Department of Histology and Embryology
School of Basic Medical Sciences
Guangdong Provincial Key Laboratory of Bone and Joint Degeneration Diseases
The Third Affiliated Hospital of Southern Medical University
Southern Medical University
Guangzhou 510515, P. R. China
E-mail: kkwu@smu.edu.cn; jsguo4127@smu.edu.cn

Y. Li
Department of Plastic and Aesthetic Surgery
Nanfang Hospital of Southern Medical University
Guangzhou 510515, P. R. China

Q. Liu, Z. Hou, Z. Lu
Regenerative Medicine and Tissue Repair Material Research Center
Huangpu Institute of Materials
Guangzhou 510530, P. R. China

The ORCID identification number(s) for the author(s) of this article can be found under https://doi.org/10.1002/smll.202205489.

DOI: 10.1002/smll.202205489

modulate the wound inflammation microenvironment,[7,17–19] regulate the phenotypes and amount of macrophages,[11,20] or inhibit the degradation of extracellular matrix (ECM) proteins[21] have been demonstrated to accelerate diabetic wound healing; oxygen therapies targeting hypoxia[2,4] and gene engineered probiotics[16] or human mesenchymal stromal cells[22] have also been reported. Although promising, most of these therapeutics only focus on one or several disconnected clues of chronic wound healing, a comprehensive strategy to facilitate the macroscopical wound closure and dressing change, protect the wounds from extrinsic threats, as well as connect the sequential wound healing phases and the cascade biological processes involving in the complex chronic wound healing, is urgently needed.

Compared with conventional dry gauze and cotton cloth dressings, new types of dressings including films, electrospun nanofibers, scaffolds, foams, hydrogels, and hydrocolloids,[7,21,23–25] can promote wound healing by providing superior flexibility and elasticity. Among them, hydrogels have attracted intensive attention because they can also perfectly fill irregular wounds and provide a favorable moist microenvironment beneficial for wound healing.[8,17,26,27] As a category of special hydrogel, tissue adhesives or adhesive hydrogels can conveniently adhere to and close/cover the wounds, avoiding the use of surgical sutures and extra damage to the wounds, thus are more promising.[8,28–30] Hydrogels especially adhesive hydrogels can also serve as local drug delivery platforms[31,32] or as media for photothermal/photodynamic therapies (PTT/PDT).[29,33–35] On the other hand, dressing changing often cause secondary injury to diabetic wounds, making wound healing even harder.[17] Therefore, fast biodegradable/absorbable,[17] on-demand dissolvable,[6,27] or painlessly removable[36,37] diabetic wound dressings, which can eliminate the destruction of a newly formed tissue during dressing exchange, have received intensive research attentions. However, effectively balancing physical properties, biological activities and on-demand removability/dissolvability of tissue adhesives to facilitate diabetic wound healing is still a big challenge.

Inspired by mussel and tannin, researchers have developed a category of tissue adhesives with strong wet adhesion to soft tissues through the introduction of catechol or galloyl species into polymer systems.[38–41] Leveraging the versatile citrate chemistry,[42] a family of injectable citrate-based mussel-inspired bioadhesives (iCMBAs) has been developed in our group via a facile one-pot polycondensation of citric acid (CA), polyol, dopamine (DP), and other functional moieties.[29,43,44] And the catechol/galloyl groups containing mussel-/tannin-inspired tissue adhesives can be oxidized or coordinated with metal ions, to give melanin-like dark-colored materials with intrinsic photothermal capability, enabling photothermal therapy (PPT) to prevent bacterial infection in diabetic wounds.[8,45–48] However, the covalent crosslinks of mussel-/tannin-inspired tissue adhesives crosslinked by oxidants (sodium periodate (PI) and silver nitrate ($AgNO_3$)) are irreversible,[43,44,49] and the degradation times of these adhesives are normally from several weeks to several months,[43,44] which is undesirable for diabetic wound healing. Benefiting from its multiple and concentrated phenolic groups, tannic acid (TA) is able to crosslink with various polymers containing hydrogen-bond donors/receptors, such as poly(ethylene glycol) (PEG),[50] poly(vinyl alcohol) (PVA),[51] and silk fibroin (SF),[52] by hydrogen bonding, the formed composites/hydrogels are sensitive to external stimuli and are possible to be designed into on-demand removable. The introduction of a strong anti-oxidant, TA, rather than toxic oxidants, is expected can further enhance the anti-oxidant activity of catechol moieties containing mussel-inspired adhesives to better deal with the severe oxidative stress of diabetic wounds.[25] In addition, TA or phenolic groups can also chelate with metal ions (such as Ag^+, Fe^{3+}, Al^{3+}, and Cu^{2+}) to form metal–phenolic networks (MPNs) or metal–phenolic coordination polymers (MPCPs).[53–56] Among metal ions, europium (Eu, a rare earth metal) ions have attracted increasing attention due to its angiogenesis promotion activity.[54,57,58] Furthermore, the metal–phenolic coordination bonds tend to disintegrate under acidic conditions caused by the competition of phenolic groups between protons and metal ions.[59] The pH-responsive metal ion release profile is beneficial for diabetic wound healing because the pH values of diabetic wounds are usually <6.5.[8,60]

In this work, utilizing the versatile bonding ability of tannin, a series of tannin–europium coordination complex (TEC) crosslinked citrate-based mussel-inspired bioadhesives (TE-CMBAs) were specially developed for convenient diabetic wound healing, via a simple physical mixing of TEC (synthesized through a facile precipitation reaction between Eu^{3+} and TA with previously developed iCMBA prepolymer)[29] (**Scheme 1**). The TE-CMBAs exhibited favorable shape adaptibility, considerable tissue adhesion, fast self-healability, pH-responsive Eu^{3+} and TA releasing properties, and advantageous on-demand dissolvability upon mixing with a mild sodium tetraborate pentahydrate (borax) solution, enabling the convenient application of TE-CMBAs for diabetic wound healing and in-time on-demand removal. In vitro studies demonstrated the favorable biocompatibility, and excellent photothermal antibacterial ability upon near-infrared (NIR) light irradiation of the adhesives. Avoiding the use of harsh strong oxidant crosslinking initiators, the inclusion of TEC into TE-CMBA further enhanced the anti--oxidant and anti-inflammatory activities. Furthermore, the wound healing efficacy of TE-CMBAs on both acute full-thickness skin wound model and diabetic chronic wound model was also thoroughly investigated. TE-CMBAs serve as a versatile multifunctional therapeutic tissue adhesive platform not only facilitating macroscopical wound closure and dressing change, but also providing smart microenvironment responsiveness and biological modulation functions, to promote diabetic wound healing.

2. Results and Discussion

2.1. Synthesis of TEC, Gelation, and Physical Properties of TE-CMBAs

From the scanning electron microscope (SEM) images of TEC shown in **Figure 1**A and Figure S1 (Supporting Information), it can be seen that the obtained TEC particles were microspheres with sizes less than 100 nm (mean size = 68.5 nm). The X-ray diffraction (XRD) spectrum of TEC (Figure 1B) displayed a broad peak similar to TA, indicating an amorphous structure.

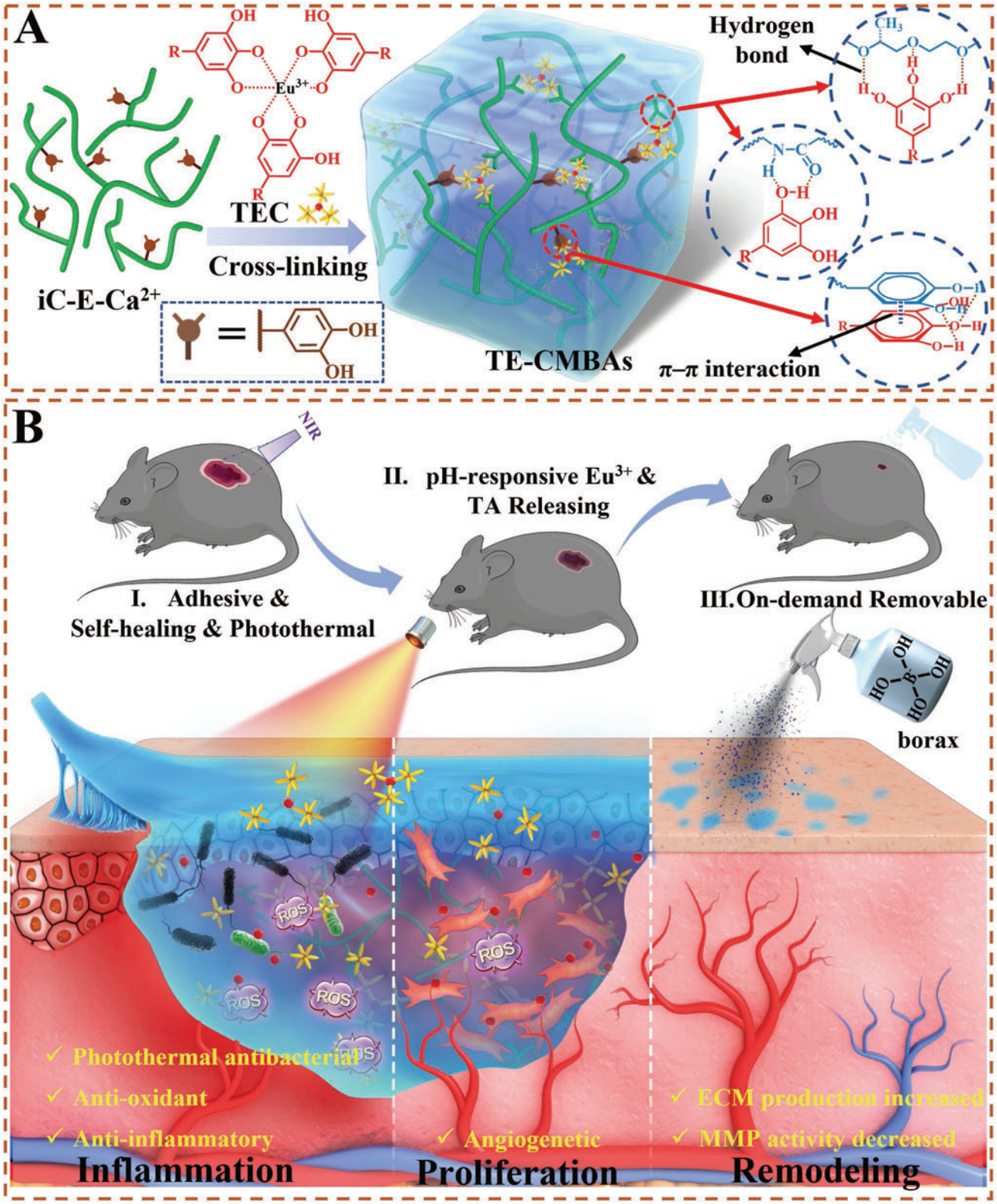

Scheme 1. A) Design strategy and fabrication of tannin–europium coordination complex (TEC) crosslinked citrate-based mussel-inspired bioadhesives (TE-CMBAs); B) Adhesive, self-healing, photothermal antimicrobial, pH-responsive europium ion (Eu^{3+}) and tannic acid (TA) releasing and on-demand removable properties of TE-CMBAs enable inflammatory microenvironment modulation and angiogenesis for accelerated diabetic wound healing.

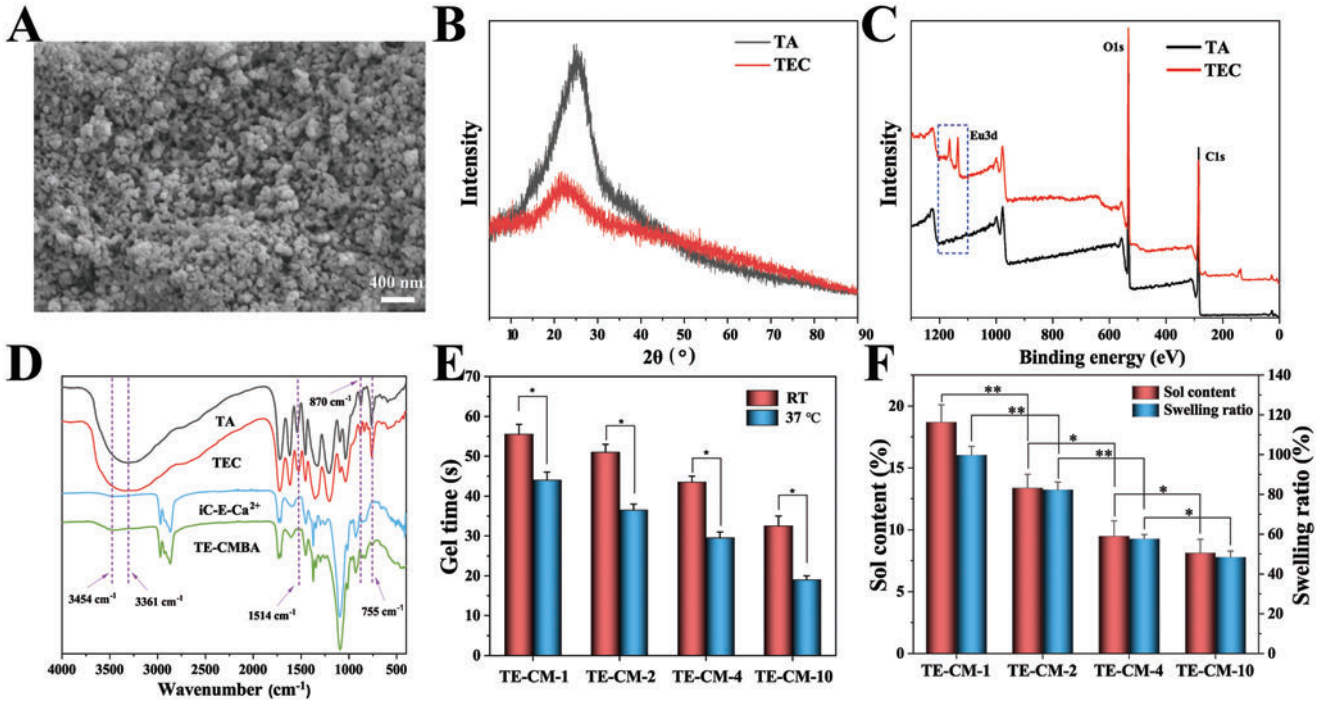

Figure 1. Characterizations of TEC and TE-CMBAs: A) SEM image of TEC; B) XRD patterns of TA and TEC; C) XPS spectra of TA and TEC; D) FTIR spectra of TA, TEC, iC-E-Ca^{2+}, and TE-CMBA; E) gel times of TE-CMBAs at room temperature (RT) and 37 °C ($n = 3$); F) sol contents and swelling ratios of TE-CMBAs ($n = 3$). $*p < 0.05$, $**p < 0.01$.

The characteristic peak of TA at $2\theta = 20°–30°$ in the XRD pattern of TEC showed an intensity decrease and a slight peak shift comparing to that of TA, which might be attributed to that the chelation between Eu^{3+} and TA reduced the amount of exposed phenolic groups in TA. The show up of both the peaks of O (532.5 eV) and C (288.1 eV) from TA, and the bimodal peaks of Eu3d (1130–1170 eV) in the X-ray photoelectron spectroscopy (XPS) spectrum of TEC (Figure 1C) confirmed the successful synthesis of TEC.[57] The Fourier transform infrared (FTIR) spectrum of TEC (Figure 1D) also displayed the characteristic peaks of ester groups (1735 cm^{-1}) and benzene rings (1450–1610, 870, 755 cm^{-1}) from TA, and the additional peak between 755 and 870 cm^{-1} (assigned to the vibration of C—H on benzene rings) showed up, further confirming the effective coordination between phenolic groups with Eu^{3+}.[54]

There are still plenty of phenolic groups derived from TA on the surface of TEC, which could be used to crosslink the $CaCO_3$ treated EPE containing iCMBA (iC-E-Ca^{2+}) prepolymer,[43] via a simple physical mixing, to obtain TE-CMBAs (Figure S2, Supporting Information). The ratios of TEC to iC-E-Ca^{2+} for TE-CMBAs with different formulations are listed in Table S1 (Supporting Information). It is deemed that the immobilized TA molecules on TEC crosslinked with iC-E-Ca^{2+} through three different interactions: hydrogen bonding between the phenolic groups of TA with the catechol groups, the ether bonds (from EPE), and the amide groups in iC-E-Ca^{2+}; π–π interactions between the phenolic groups of TA with the catechol groups in iC-E-Ca^{2+}; hydrophobic interaction (Scheme 1A).[61] Upon the physical mixing of TEC with iC-E-Ca^{2+}, gelation was instantly formed in less than 1 min (35–55 s) at room temperature, which was attributed to the rapid formation of hydrogen bond between TEC and iC-E-Ca^{2+} (Figure 1E). Higher TEC contents led to faster crosslinking, and the gelation was further sped up when the temperature was increased to 37 °C. The formation of hydrogen bonds was confirmed by the peak shift of the free phenolic hydroxyl groups in TA at 3361 cm^{-1} to the related hydrogen bonds at 3454 cm^{-1} as shown in the FTIR spectra (Figure 1D).[62] All the tested TE-CMBA formulations exhibited low sol contents (<20%) and appropriate swelling ratios (40%–100%) (Figure 1F), and they all decreased with the increase of TEC contents. Suitable swelling of TE-CMBAs enables TE-CMBAs to absorb wound exudate and maintain a moist microenvironment, beneficial for granulation and epithelial tissue regeneration during wound healing.

2.2. Mechanical and Tissue Adhesion Properties of TE-CMBAs

Suitable elasticity and mechanical stability of material are beneficial for skin wound healing, to maintain the integrity of the material when the skin tissue is deformed by an external force.[63] As shown in **Figure 2**A, both the un-crosslinked iC-E-Ca^{2+} prepolymer and the crosslinked TE-CMBAs exhibited excellent elasticity. The tensile strengths of all tested TE-CMBAs were >400 kPa (Figure 2B). And the tensile strength increased with the increase of TEC content, the Young's moduli of TE-CMBAs showed the same trend (Figure S3, Supporting Information). However, the elongation at break decreased with the increase of TEC content (Figure S4, Supporting Information). The inclusion of TEC significantly improved the elasticity and mechanical stability of TE-CMBAs compared to that of un-crosslinked iC-E-Ca^{2+}, proved the effective crosslinking of TEC

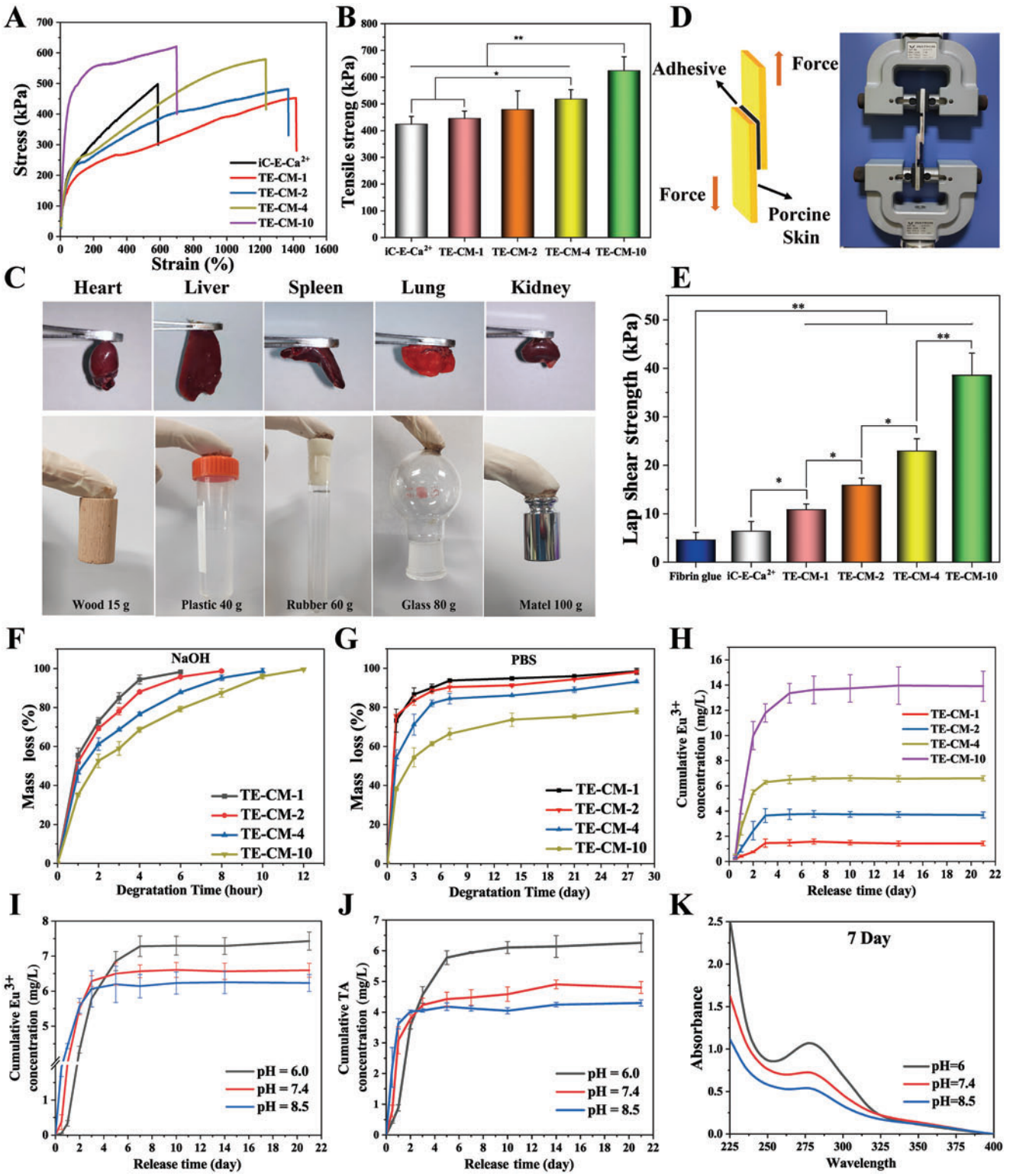

Figure 2. Mechanical, adhesive, degradation, and pH-responsive release properties of TE-CMBAs: A) representative stress–strain curves of TE-CMBAs; B) tensile strengths of TE-CMBAs ($n = 5$); C) photographs of TE-CMBAs adhered to wet tissues and different material substrates; D) diagram of lap shear strength test of the adhesive to porcine skin tissue; E) lap shear strengths of TE-CMBAs to porcine skin ($n = 4$); degradation profiles of TE-CMBAs in F) 2 M NaOH solution and G) PBS (pH = 7.4) ($n = 3$); H) the cumulative Eu^{3+} concentrations released from different TE-CMBAs ($n = 3$); the cumulative concentrations of I) Eu^{3+} and J) TA in solutions with different pH values ($n = 3$); K) the absorbance of TA released in solutions with different pH values on the seventh day ($n = 3$). $^{*}p < 0.05$, $^{**}p < 0.01$.

to iC-E-Ca^{2+} prepolymer once again. Moreover, the mechanical properties of TE-CMBAs in hydrated status were also studied. Although the mechanical strengths decreased for all the tested samples at wet condition, considerable elasticity was kept, ensuring the effective use of TE-CMBAs at diabetic wound sites (Table S2, Supporting Information). Wound dressing with sufficient adhesive property can eliminate the use of surgical suture, avoiding secondary injury and facilitating wound healing.[25,8,37] Thus, the adhesion property of TE-CMBAs was studied, the results are shown in Figure 2C–E. TE-CMBAs showed strong adhesion to fresh wet tissues, such as the heart, liver, spleen, lung, and kidney; TE-CMBAs could also adhere to various other substrates, including wood, plastic, rubber, glass, and metal, indicating their wide applicability (Figure 2C). Moreover, the adhesion ability of TE-CMBAs to wet tissues was quantitatively evaluated through lap shear strength tests using porcine skin as a biological tissue model (Figure 2D). The adhesion strengths of all the tested TE-CMBA formulations were significantly higher ($p < 0.01$) than that of commercially available fibrin glue (4.58 ± 1.57 kPa), the gold standard of tissue adhesives. And with the increase of TEC content, the adhesion strength TE-CMBA to wet tissue gradually increased from 10.8 to 38.5 kPa (Figure 2E). The adhesion strength of un-crosslinked iC-E-Ca^{2+} was significantly lower than that of TE-CMBAs, and similar with that of fibrin glue, indicating the importance of TEC crosslinking in the improvement of the adhesion strengths. The adhesion mechanism of TE-CMBAs to wet tissue is deemed mainly caused by the presence of a large amount phenolic groups derived from both DP and TA, which enabled TE-CMBAs to bond to various substrates through noncovalent bonding (hydrogen bonding, electrostatic interaction, hydrophobic interaction, and π/cation–π stacking), and even covalent bonding between phenolic groups and amino/thiol groups of proteins on the tissue surface.[25,8,64] The inclusion of TEC not only enhanced the cohesion by providing metal–phenolic coordination as well as hydrogen bonding and π/cation–π stacking between TEC and iC-E-Ca^{2+} but also improved the interfacial adhesion to biological surfaces by providing surface adhesion between the residual phenolic groups and the tissue surface. The existence of rigid TEC particles in flexible polymer network of the crosslinked TE-CMBAs balanced the good interfacial adhesion and strong internal adhesion, together contributing to the excellent tissue adhesion strength.

2.3. Degradation Profiles and pH-Responsive Release of Eu^{3+} and TA

As shown in Figure 2F, all the tested TE-CMBAs completely degraded in 12 h in 2 M NaOH solution, and TE-CMBAs with higher TEC contents degraded slower. The degradation of TE-CMBAs in PBS exhibited a "first fast then slow" phenomenon with more than 35% degradation being reached in only 1 d (Figure 2G), once more confirming the weak hydrogen bond crosslinking between TEC and iC-E-Ca^{2+}. While, for TE-CM-10, only ≈66% degradation was reached in one week, and ≈25% of the adhesive was still left after 28 days' degradation, indicating a considerable stability of TE-CMBAs especially at high TEC contents. Along with the degradation of TE-CMBAs, Eu^{3+} continually released and showed a three-phase release profile: an initial rapid release, a lag phase slow release, and a final steady release (Figure 2H). The final cumulative Eu^{3+} release amounts from TE-CMBAs were in proportion to the TEC contents, exhibiting a dose-dependent release profile, and the release curves were basically consistent with the degradation curves.

Diabetic wounds have a high glucose level, which can easily lead to a high inflammatory reaction, bacterial colonization, and multiplication, making the pH of the wound surface acidic (usually <6.5).[60,65] As a kind of MPN, TEC was reported to possess pH-responsive dissociation property,[54] therefore, the Eu^{3+} and TA release profiles from TE-CMBAs at different pH values were investigated. As shown in Figure 2I, in the initial 3 d, the release of both Eu^{3+} from TE-CMBAs at basic pH values (7.4 and 8.5) was faster than that at acidic pH (6.0). While the total release amounts of Eu^{3+} after 21 d increased with the decrease of pH, the cumulative release concentrations of Eu^{3+} were 5.8 mg L^{-1} (pH 8.5), 6.5 mg L^{-1} (pH 7.4), and 7.2 mg L^{-1} (pH 6.0), respectively; and the time reaching an equilibrium phase were also extended from 3 d (pH 8.5), 5 d (pH 7.4) to 7 d (pH 6.0) (Figure 2I). The release of TA at different pH, calculated by the UV absorbances according to the TA standard curve (Figure 2K and Figure S5, Supporting Information), exhibited a similar trend with that of Eu^{3+} (Figure 2J). The initial faster release of Eu^{3+} and TA at alkaline conditions was believed to be caused by the weakened hydrogen bonds between TEC and iC-E-Ca^{2+} at basic pH conditions led to relatively faster rapid release of TEC from TE-CMBA networks (Figure S6, Supporting Information). However, at acidic pH, the competition of phenolic groups between protons and metal ions made the metal–phenolic coordination in TEC weaker and easily dissociable, leading to longer duration and more cumulative Eu^{3+} and TA release from TE-CMBAs (Figure S6, Supporting Information). On the other hand, at acidic pH, most phenolic hydroxyl groups on iC-E-Ca^{2+} were also protonated, they would also compete the binding sites on TA with metal ions, further sped up the release of Eu^{3+} and TA from TE-CMBAs.[59] The favorable pH-responsive release of Eu^{3+} and TA facilitate the application of TE-CMBAs in the acidic microenvironment of diabetic wounds, to promote angiogenesis and modulate the inflammatory microenvironment, thus can accelerate diabetic wound healing.

2.4. Shape Adaptability, Self-Healability, and On-Demand Removal Ability of TE-CMBAs

The ideal adhesive dressing should be easily adapted to versatile shapes and sizes, conveniently apply to any irregularly shaped wound and be self-healable, to act as a smart physical barrier against external stimulation.[25] As shown in **Figure 3**A, TE-CMBAs can easily fill the star-shaped teflon mold in 15 min, exhibiting a favorable shape-adaptability. As depicted in Figure 3B, when the cut TE-CMBA disks contacted each other, the rearrangement of hydrogen bonds (as shown in the lower panel of Figure 3B) could promote the fast self-healing of the hydrogels immediately (fused in 2 min).[25] The mechanical properties of the fused adhesive did not change much

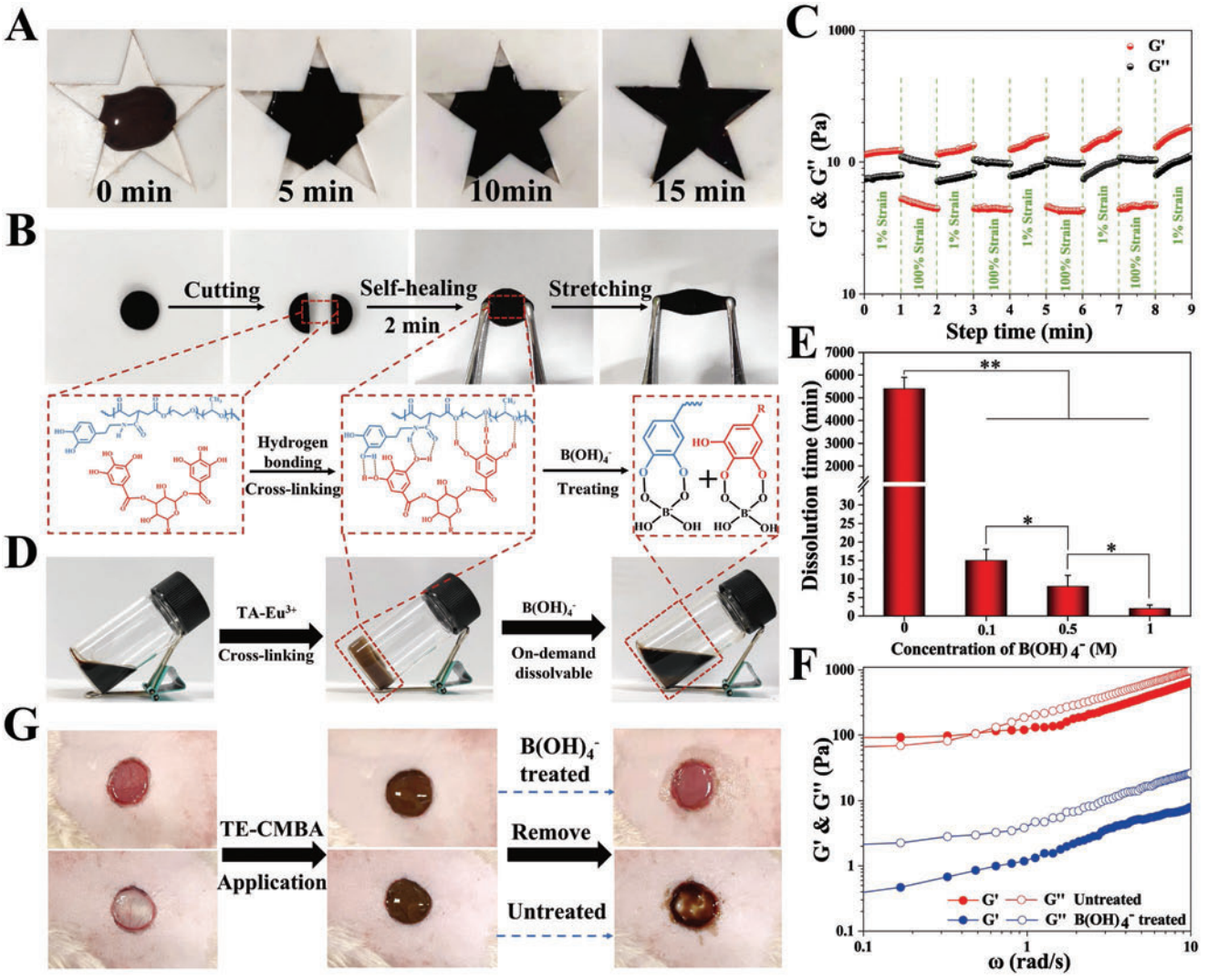

Figure 3. Shape adaptive, self-healing, and on-demand removable functionalities of TE-CMBAs: A) shape-adaptive performance and B) macro self-healing property and mechanism of TE-CMBAs; C) rheological properties of TE-CMBA (TE-CM-4) when the step strain was alternately switched from 1% to 100%; D) the dissolution behavior of TE-CMBAs upon mixing with borax ($NaB(OH)_4$) solution; E) the effect of $B(OH)_4^-$ concentration to dissolution time of TE-CM-4 ($n = 3$); F) rheological analysis of the TE-CM-4 treated/untreated with borax solution; G) the in vivo experiment demonstrating the on-demand removal of TE-CMBA from full-thickness skin wound after borax solution treatment. $^*p < 0.05$, $^{**}p < 0.01$.

comparing the original adhesive (Figure S7, Supporting Information), further confirming the favorable self-healing ability of TE-CMBAs. From the oscillatory step strain recovery experiment results shown in Figure 3C, it can be seen that after relaxation (strain = 1%) for 1 min following 1 min of subjection to a large strain (100%) shear, the storage moduli (G') of TE-CM-4 could be fully restored even after four cycles. The excellent self-healability of TE-CMBAs was attributed to the flexibility and the high elasticity of iC-E-Ca^{2+} as well as the highly dynamic reversible hydrogen bonds between TEC and iC-E-Ca^{2+}. The shape-adaptable and fast self-healing features confer TE-CMBAs the abilities to automatically change shape to match the irregular diabetic wounds, and to quickly response to possible dressing break by normal body movement and local stress, which are beneficial for the prevention of external infection and the maintenance of a sterile environment for wound healing.

A painless and on-demand removable or dissolvable ability is one of the most favorable functions of wound dressings for their convenient clinical applications, especially in hard-to-heal wounds such as diabetic wounds.[6,34] As shown in Figure 3D, TE-CMBA (using TE-CM-4 as the representative) dissolved upon mixing with appropriate amount of borax solution. With the increase of borax concentrations from 0.1, 0.5 to 1.0 mol L^{-1}, the dissolution times of TE-CM-4 quickly decreased from ≈15, ≈6 to ≈1.5 min (Figure 3E). While, without borax ($B(OH)_4^-$) solution, it needed more than 3 d (≈5500 s) to dissolve TE-CM-4 in deionized water (Figure 3E). The effect of borax on the mechanical properties of TE-CMBAs was further evaluated by rheological test. From Figure 3F, it can be seen that although TE-CM-4 showed a shear-thinning feature, the storage moduli (G') were still higher than that of loss moduli (G'') at low frequency, which is a characteristic of hydrogel.

However, after being treated with borax solution, the G' and G'' significantly decreased, and showed a liquid property ($G'' > G'$) within the whole tested frequency range (Figure 3F). It is deemed that the hydrogen bonds between iC-E-Ca^{2+} and TEC in TE-CMBAs were destroyed and replaced by the boric acid ester bonds between catechol or galloyl groups and borax (as shown in the lower panel of Figure 3D), making the polymer dissolvable and easily removable.[6,66] The fast dissolution of TE-CMBAs by borax solution makes TE-CMBAs a convenient on-demand removable wound dressing, greatly beneficial for their application in wound healing, which was further verified in a full-thickness skin wound mold. As shown in Figure 3G, compared with the untreated TE-CMBA, after being treated with borax, the adhesive could be easily wiped leaving nearly no residual adhesive on the wound. The three-dimensional network of TE-CMBAs will degenerate with the addition of borax, forming removable adhesive that can be dissolved on demand, alleviating the trouble of changing wound dressings and eliminating secondary injuries caused by invasive wound dressing change.

2.5. Photothermal and Photothermal Antibacterial Properties of TE-CMBAs

The photothermal property of TE-CMBAs was evaluated via recording the temperature change (ΔT) under 808 nm NIR irradiation. As shown in **Figure 4**A, for all tested samples, a fast temperatures rise was observed in the first 5 min, then the temperature rise slowed down and entered into a platform stage. The iC-E-Ca^{2+} prepolymer exhibited considerable photothermal ability itself, and the inclusion of TEC further reinforced the photothermal efficacy of TE-CMBAs, higher TEC content led to higher temperature rise (ΔT) (Figure 4A). This phenomenon implied that the photothermal ability of TE-CMBAs comes from both the catechol groups of iC-E-Ca^{2+} and galloyl groups of TA, and the coordination of galloyl-Eu^{3+} might also promote the efficiencies of NIR light absorption and thermal conversion.[46] Also, the photothermal properties of the TE-CMBAs with different irradiation power densities were studied using TE-CM-4 as a representative sample. Higher NIR power density led to faster and higher temperature rise (Figure 4B). At the end

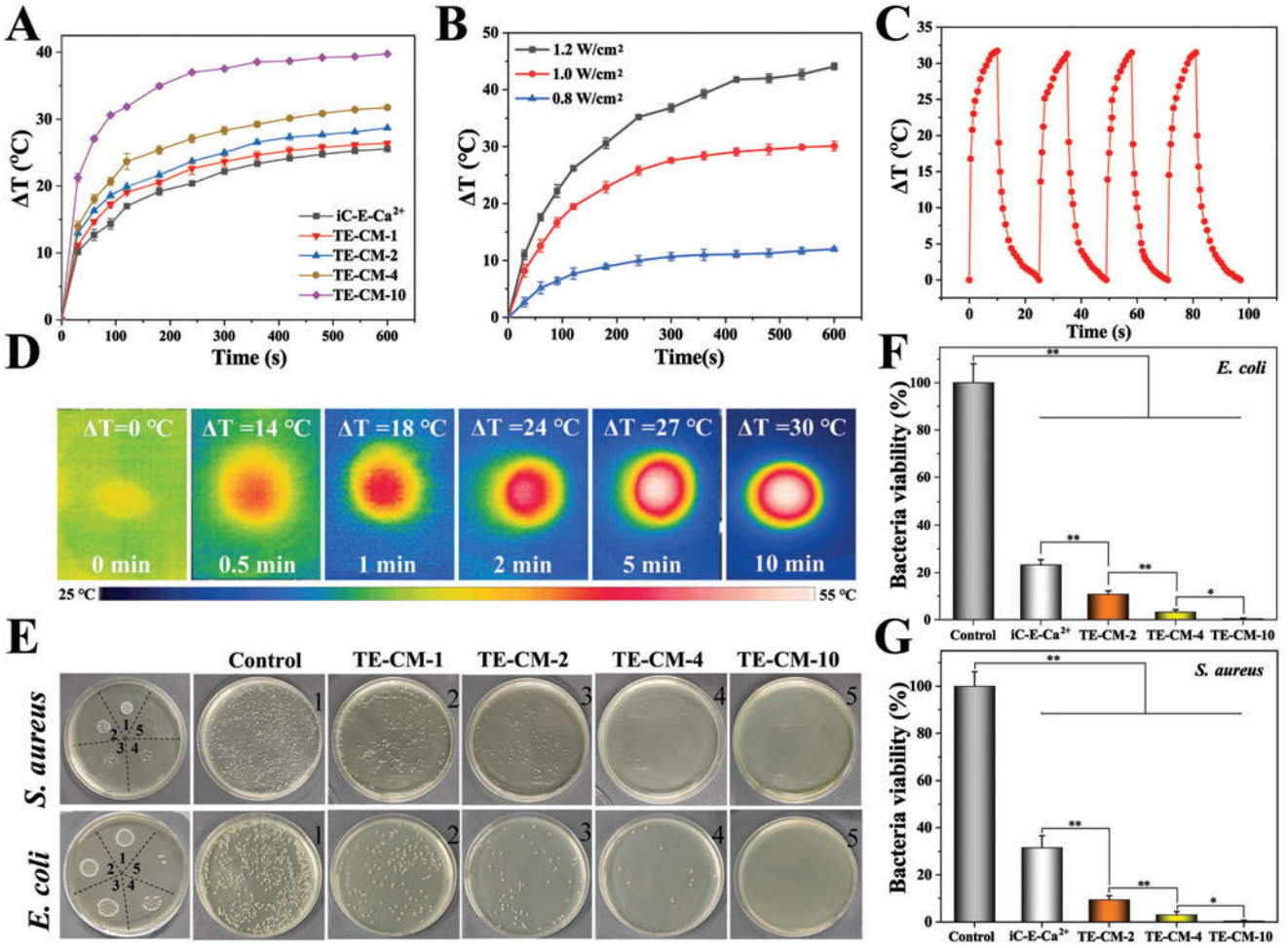

Figure 4. Photothermal property and photothermal antibacterial activity of TE-CMBAs: A) the ΔT-NIR irradiation time curves for different TE-CMBAs at a power density of 1.0 W cm^{-2}; B) the ΔT-NIR irradiation time curves for TE-CM-4 under NIR with different power densities; C) temperature change curve of TE-CM-4 over four NIR irradiation on/off cycles (power density = 1.0 W cm^{-2}); D) thermographic images of TE-CM-4 under NIR irradiation at a power density of 1.0 W cm^{-2}; E) the macroscopic photos of survival bacterial colonies; the bacterial viabilities of F) *S. aureus* and G) *E. coli* after exposed to TE-CM-4+NIR irradiation (1.0 W cm^{-2}) for 10 min ($n = 3$). $^*p < 0.05$, $^{**}p < 0.01$.

of 10 min NIR irradiation, ΔT was 45 °C at 1.2 W cm^{-2}, 30 °C at 1.0 W cm^{-2}, and 12 °C at 0.8 W cm^{-2}, respectively. Moreover, TE-CMBAs also exhibited highly repeatable photothermal ability, which can be seen from that TE-CM-4 maintained the same temperature increase trend and the highest ΔT was kept without any attenuation after four consecutive NIR irradiation (1.0 W cm^{-2}) and free cooling cycles (Figure 4C). At the same time, as reflected in the heatmaps shown in Figure 4D, the heating zone in TE-CMBA (using TE-CM-4 as the representative) was well limited to the laser-irradiated spot. The fast-temperature rise, low thermal diffusion, and precise heating zone control of TE-CMBAs facilitate their photothermal application and are beneficial to avoid any undesired damage to surrounding tissues/organs when used.

One of the main reasons for the difficulty of diabetic wound healing is that diabetic wounds are vulnerable to bacterial infection,[17] necessitating the introduction of antimicrobial function in diabetic wound dressings by including antimicrobial agents or leveraging photothermal therapy (PPT) or other antimicrobial strategies. A preliminary study using TE-CMBAs to treat bacteria showed that TE-CMBAs exhibited weak inherent antibacterial ability, derived from both citric acid and TA, against *Staphylococcus aureus* (*S. aureus*) and *Escherichia coli* (*E. coli*) (Figure S8, Supporting Information).[41,42,48,67] Benefiting from their favorable photothermal ability, upon NIR irradiation, TE-CMBAs showed strong antibacterial activity significantly better than the control and iC-E-Ca^{2+} groups, which might be caused by the deformation of certain enzymes and proteins in bacteria as well as the destruction of the bacterial structure at temperatures above 50 °C (Figure 4E–G).[29] The viabilities of *S. aureus* and *E. coli* for TE-CM-2, TE-CM-4 and TE-CM-10 groups were all less than 15% after 10 min NIR irradiation (808 nm, 1.0 W cm^{-2}, Figure 4F,G). Moreover, with the increase of TEC content, the antibacterial activity was significantly enhanced, there were nearly no bacteria colonies observed in the TE-CM-4 and TE-CM-10 groups for both *S. aureus* and *E. coli* (Figure 4E–G). These results indicated that TE-CMBAs possess a favorable NIR photothermal antibacterial activity against both Gram-positive (*S. aureus*) and Gram-negative bacteria (*E. coli*).

2.6. Anti-oxidant Activity of TE-CMBAs

Excessive ROS was produced in diabetic wound sites due to long-term inflammation and bacterial infection, resulting in lipid peroxidation, DNA damage, and enzyme inactivation, thus hindering wound healing.[18,68,69] The phenolic groups from both mussel-inspired dopamine and TA molecules have been reported to possess excellent anti-oxidant ability.[25,44] The anti-oxidant activity of TE-CMBAs was estimated by measuring their scavenging efficiency to DPPH free radicals. As shown in **Figure 5**A,B, iC-E-PI crosslinked by sodium periodate (PI) possessed nearly no anti-oxidant activity due to the inclusion of a strong oxidant (PI) counterbalanced the anti-oxidant activity of iC-E-Ca^{2+}.[8,41,48] While, TE-CMBAs exhibited enhanced anti-oxidant activity compared to that of iC-E-Ca^{2+}, and the DPPH scavenging efficiencies of TE-CMBAs showed a TEC content-dependent manner, the DPPH scavenging percentages increased significantly with the increase of TEC content (Figure 5A,B). Within 5 min, the DPPH scavenging percentage reached 77% for the TE-CM-10 group, while the TE-CM-1 group only reached 43.34%. Along with time extension to 15 min, the DPPH scavenging percentage of TE-CM-4 also increased to >90% (Figure 5C,D). Furthermore, a ROS test kit was conducted to investigate the cellular anti-oxidant capacity of TE-CMBAs using mouse fibroblasts (L929), in which a Rosup agent was used to stimulate the production of excessive intracellular ROS by L929 cells, with dichlorofluorescein-diacetate (DCFH-DA) as a ROS probe. As shown in Figure 5E,F, the DCFH fluorescence intensities of TE-CMBAs treated cells were significantly lower than that in the blank and the positive control (Rosup) groups. And higher TEC content led to better intracellular anti-oxidant capacity. These results proved that TE-CMBAs possess excellent anti-oxidant capacity, making them competitive candidates to scavenge excessive ROS in diabetic wounds and promote wound healing.

2.7. In Vitro Cell Cytocompatibility, Cell Proliferation, Migration, and Tube Formation

The cytocompatibility of Eu^{3+} and TEC was evaluated via cell counting kit-8 (CCK-8) assay against L929. It can be seen from Figure S9 (Supporting Information), Eu^{3+} showed almost no toxicity to L929 at concentrations ≤85 μg mL^{-1}, the cell viabilities of Eu^{3+} at 340 and 170 μg mL^{-1} were also higher than 60%. For TEC, as shown in Figure S10 (Supporting Information), when the concentrations were <50 μg mL^{-1}, the cell viabilities of L929 were all higher than 80%. These results indicated that Eu^{3+} and TEC are cytocompatible in a reasonable range, in accordance with the cytocompatibility results of europium hydroxide nanorods[56] and other MPNs.[70]

The cytocompatibility of TE-TCMBAs was evaluated by investigating the cytotoxicity of the sol contents and degradation products of TE-TCMBAs via CCK-8 and Live/Dead assay against L929 and human umbilical vein endothelial cells (HUVECs). As shown in **Figure 6**A,B, except for TE-CM-10, the cell viabilities of HUVECs and L929 cells co-cultured with the sol contents of TE-CMBAs with different dilutions (1×, 10×, and 100×) were all >80%, indicating a favorable cytocompatibility. Although the 1× degradation products of TE-CMBAs induced significant cytotoxicity to both L929 and HUVECs (cell viabilities < 20%), 10× and 100× degradation products of TE-CMBAs showed nearly no cytotoxicity and could even promote cell growth for some formulations (Figure 6C,D). Furthermore, HUVECs were cultured with the 10× degradation products of TE-CMBAs for 1, 3, and 5 d, and studied with Live/Dead assays and CCK-8. From Figure 6E, it can be seen that HUVECs showed a spreading morphology in all tested groups, and grew faster in TE-CMBA groups and reached a cell confluence and overlap state on day 5. The cell amounts of TE-CMBAs groups were significantly higher than that of the control group, and higher TEC contents led to higher cell amounts with the cell viability of TE-CM-10 on day 5 being reached 161.42% (Figure 6F). Furthermore, the effect of TE-CMBAs on the cell migration ability was assessed by cell scratch assay and transwell experiment. As shown in Figure 6G,H the cell migration rates of TE-CMBA groups were significantly higher than that of the blank group (≈25% after

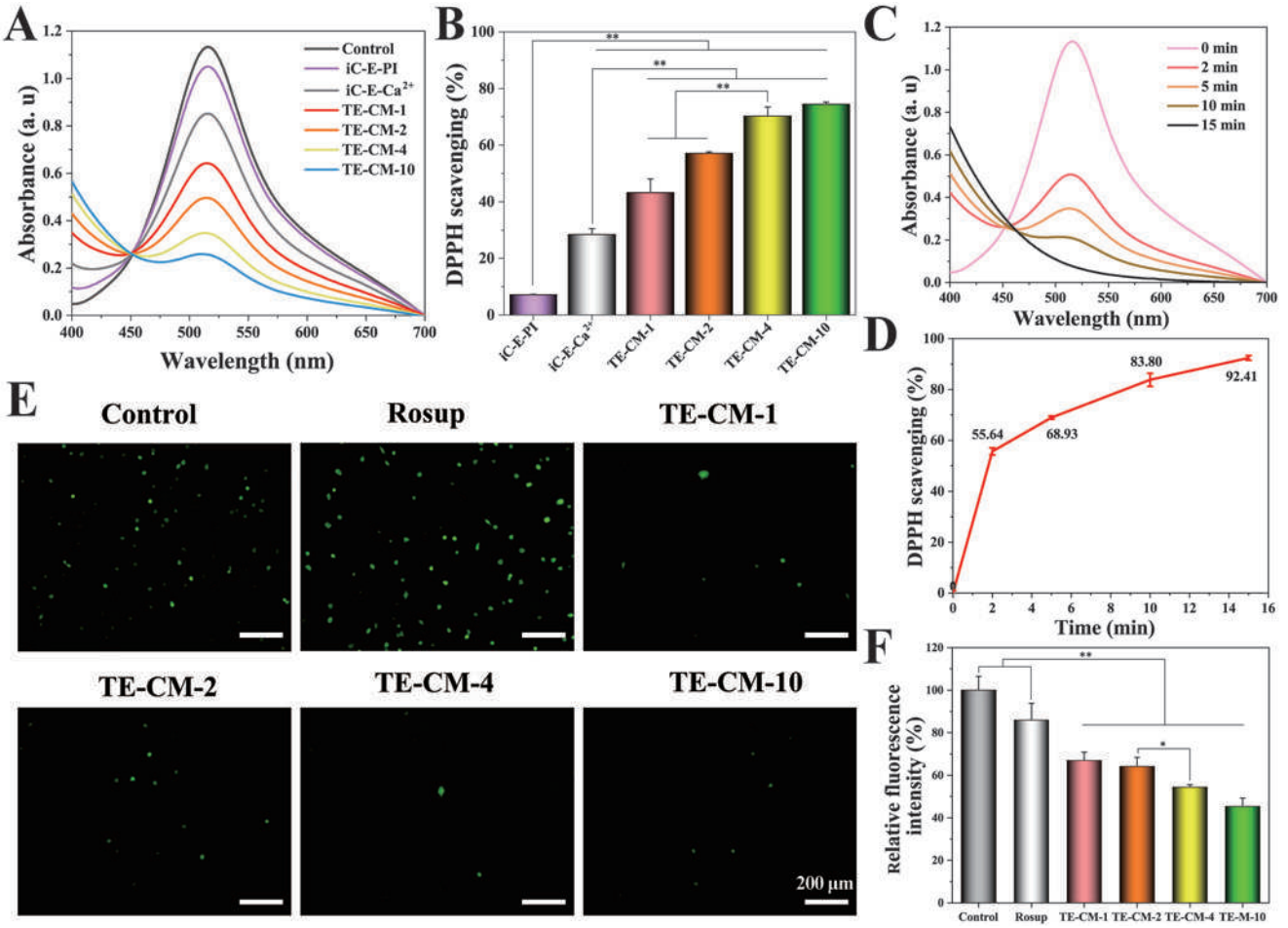

Figure 5. Anti-oxidant activity of TE-CMBAs: A) UV–vis spectra and B) DPPH scavenging percentages after incubating for 5 min ($n = 3$); C) dynamic DPPH scavenging percentages and D) UV–vis curves of TE-CM-4; E) the fluorescence images and F) relative fluorescence intensities of oxidation inhibition obtained by ROS test kit on L929 ($n = 3$). *$p < 0.05$, **$p < 0.01$.

24 h), and with the increase of TEC contents in TE-CMBAs, the cell migration rate increased from ≈37% for TE-CM-1, ≈45% for TE-CM-2, to ≈60% for both TE-CM-4 and TE-CM-10 after 24 h, implying that TA and Eu^{3+} contributed to the enhanced cell migration and proliferation. The cell migration promotion ability was further confirmed by the transwell experiment (Figure 6I,J). These results indicated that TE-CMBAs possess excellent cytocompatibility, and can significantly promote cell proliferation and migration, which is beneficial for their application in diabetic wound healing.

The vascular network reconstruction in the early stage of wound healing is very important.[13] Therefore, the angiogenetic property of TE-CMBAs was evaluated via an in vitro tube formation assay using HUVECs. As can be seen from Figure 6K, after HUVECs were treated with 10× degradation products for 6 h, more tubular structures can be observed in TE-CMBA groups than that of the control and iC-E-Ca^{2+} groups, and the TE-CM-4 group showed the densest tubular network formation. Moreover, from the relative tube lengths measured and calculated by Image J (using the average tube length of the control group as 100%), it can be seen that the TE-CMBAs groups had significantly larger tube lengths than that of the control and iC-E-Ca^{2+} groups, with the relative tube length of the TE-CM-4 group the largest (Figure 6L). These results confirmed the angiogenetic property of TE-CMBAs is mainly derived from the inclusion of Eu^{3+} and TA, both of which can promote endothelial cell proliferation and vascular germination.[54,57,58] The favorable angiogenetic property of TE-CMBAs, along with their distinctive pH-responsive Eu^{3+} and TA releasing profile making them fit well with the weak acidic diabetic wounds (pH < 6.5),[26,60] to promptly accelerate angiogenesis in the early stage of diabetic wound healing.

2.8. In Vivo Evaluation

2.8.1. In Vivo Diabetic Wound Healing Performance

In vitro studies well demonstrated the tissue adhesive, self-healing, photothermal and photothermal antimicrobial properties, favorable anti-oxidant activity and pH-responsive Eu^{3+} and TA releasing profiles, as well as on-demand removability of TE-CMBAs, all strongly suggested their great application potential in diabetic wound healing. Thus, the chronic wound

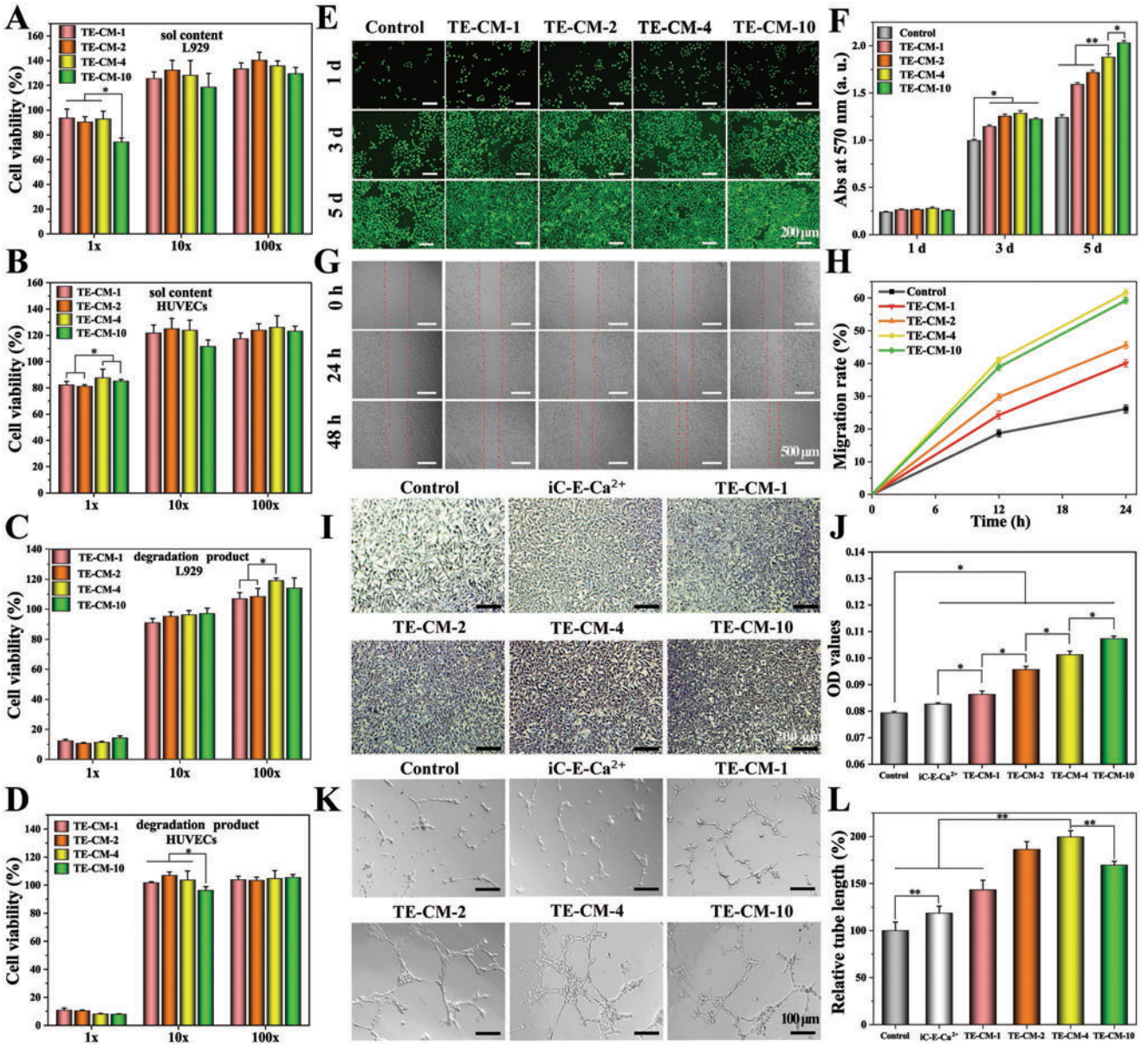

Figure 6. In vitro cytocompatibility, cell migration, and angiogenetic properties: A,B) cell cytotoxicity of sol contents and C,D) degradation products of TE-CMBAs against L929 and HUVECs for 24 h ($n = 3$); E) representative Live/Dead images and F) quantitative cell amounts of HUVECs after incubating with 10× degradation products of TE-CMBAs for 1, 3, and 5 d ($n = 3$); G) cell migration images and H) quantitative cell migration rates obtained by L929 cell scratch test ($n = 5$); I) representative images and J) quantitative OD values of L929 cells transwell migration assay after being cultured with 10× degradation products of TE-CMBAs for 24 h ($n = 3$); K) representative in vitro tube formation images and L) relative tube lengths of HUVECs after being co-cultured with 10× degradation products of TE-CMBAs for 6 h ($n = 3$). $^*p < 0.05$, $^{**}p < 0.01$.

healing efficacy of TE-CMBAs (using TE-CM-4 as the representative) was assessed using a full thickness wound model on type 2 diabetic db/db (Leprdb/db) mice (**Figure 7**A and Table S3, Supporting Information). The acute wound healing performance of TE-CM-4 was also studied for comparison, using a full thickness wound model on wild mice (C57BL/6). The average blood glucose concentration of the used diabetic db/db mice was determined to be 29.0 ± 4.0 mmol L^{-1}, conforming to the characteristics of diabetic mice (Table S3, Supporting Information).[71] The successful establishment of type 2 diabetic db/db mice model was further confirmed by the show up of serious diabetic complications represented in the hematoxylin and eosin (H&E) staining images, including liver damage with obvious fatty accumulation as well as kidney enlargement with kidney tubule hypertrophy and basement membrane thickening (Figure 7A). The diabetic db/db mice also had a significantly thicker subcutaneous fat layer and much larger adipocytes comparing to C57BL/6 mice (Figure 7A). The pH value of tissue on the diabetic wound site was measured to be 6.25 ± 0.25 (the pH of the built acute wound tissue was 7.25 ± 0.25) (Table S3, Supporting Information), in accordance with previous literature.[26,60]

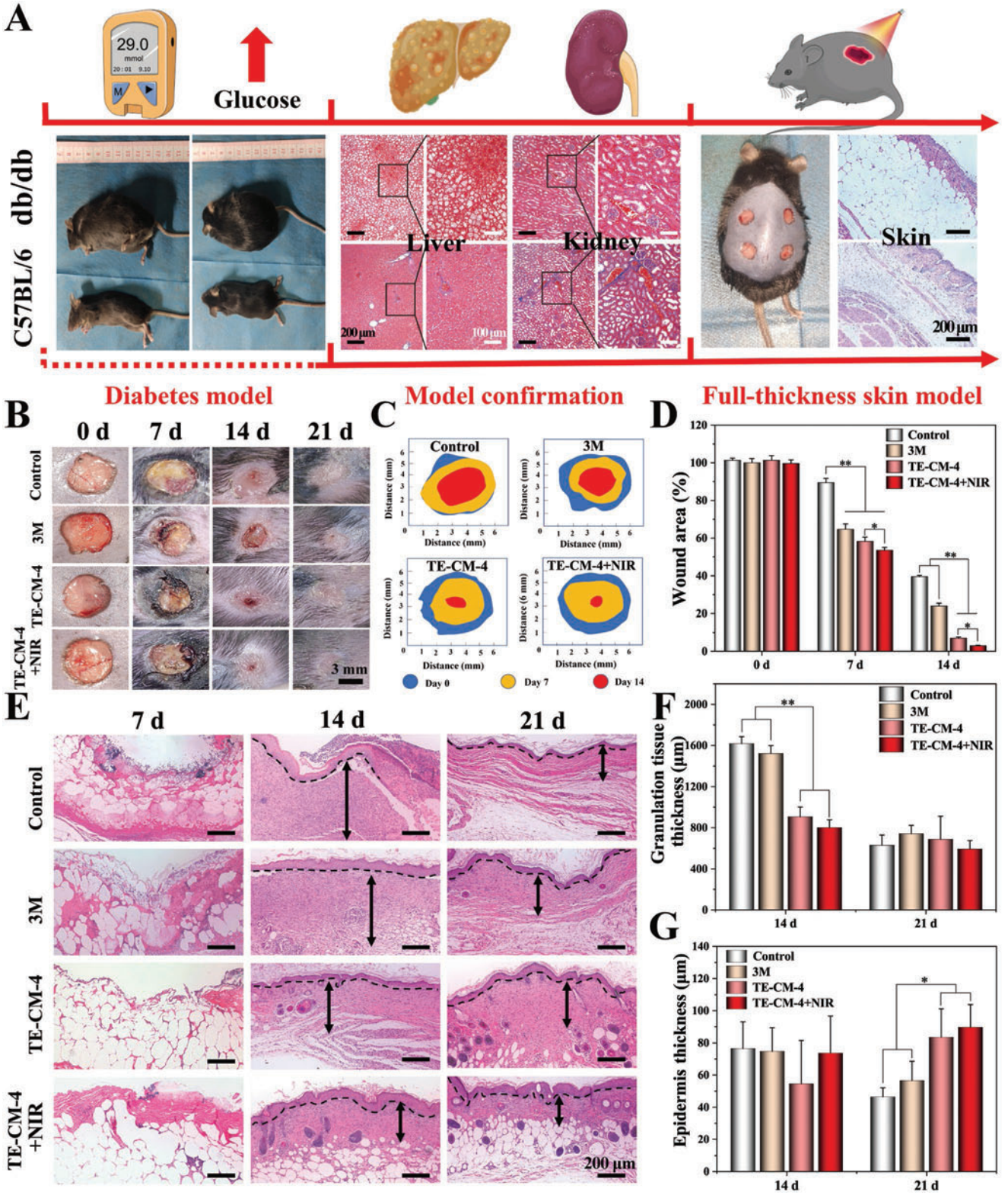

Figure 7. Wound closure results of diabetic wounds: A) establishment of diabetic db/db mice model confirmed with hematoxylin and eosin (H&E) staining of liver, kidney, and skin, and the comparison to C57BL/6 mice model; B) representative photographs of diabetic wounds for the control, 3 M Tegaderm film, TE-CM-4 and TE-CM-4+NIR groups on the 0, 7th, 14th, and 21st day; C) schematic diagram of wound closure and D) quantitative analysis of wound area change in comparison with the original wound ($n = 5$); E) representative H&E staining images of treated skin tissues on the 7th, 14th, and 21st day postsurgery (Arrow: granulation tissue thickness; dotted line: epidermis and dermis dividing line); quantitative data of F) granulation tissue thickness and G) epidermis thickness on the 14th and 21st day after operation ($n = 5$). $^{*}p < 0.05$, $^{**}p < 0.01$.

The photothermal temperature change images of diabetic wounds treated with TE-CM-4+NIR are shown in Figure S11 (Supporting Information). The temperature of the diabetic wound-site in the TE-CM-4+NIR group rapidly increased within 10 min, and the heating zone was well confined within the adhesive spot irradiated by the laser, consistent with the in vitro results. To match the Eu^{3+} and TA releasing properties of TE-CM-4 with wound healing timeline, TE-CM-4 and commercially available 3 M Tegaderm film (as positive control) were changed every 7 d in the initial stage of healing. Benefiting from its on-demand dissolvability/removability (Figure 3G), TE-CM-4 could be conveniently removed by adding an appropriate amount of borax solution, to avoid secondary injury. Representative wound closure photographs of the diabetic wounds treated by different samples are shown in Figure 7B. No obvious wound contraction was found on the seventh day post treatment, and residual scabs (crusts of dried blood, serum, and exudate) could be still observed on the 14th day, especially for the control group; the healing rates of chronic diabetic wounds (Figure 7B–D) were significantly slower than that of acute wounds (Figure S12A–C, Supporting Information), validating the delayed healing characteristic of diabetic wounds. This might be caused by the thick subcutaneous fat layer and the lack of epithelial cells in diabetic wounds, as well as persistent inflammatory reaction that impeded normal wound contraction process driven by surrounding skin tissue. Although difficult to heal, the administration of TE-CM-4 with/without NIR irradiation led to significantly accelerated diabetic wound closure comparing to the control and 3 M groups, especially on day 14 (Figure 7B–D), exhibiting a similar trend as seen in the acute wound healing case where a primary wound closure occurred on day 7 (Figure S12, Supporting Information).The relative unhealed wound areas were 7.0 ± 0.56% and 2.9 ± 0.2% for TE-CM-4 and TE-CM-4+NIR groups, respectively, significantly lower than that of the control (39.5 ± 0.6%) and 3 M (23.9 ± 1.5%) groups (Figure 7D). The accelerated wound healing induced by TE-CM-4 and TE-CM-4+NIR groups can also be reflected by the fact that as early as on the seventh day, the granulation tissue in the TE-CM-4 group was crawling toward the center of the wound, and reestablishment of epithelial continuity was already realized for the TE-CM-4+NIR group, but the subcutaneous fat layer had necrotized and the epithelial cells hardly proliferated in the control and 3 M groups (Figure 7B,E and Figure S13, Supporting Information). The wound healing promoting effect of TE-CM-4 or TE-CM-4+NIR can also be reflected from the relatively complete and well-organized epidermis layers of the adhesive groups comparing to that of the control and 3 M groups in the case of acute wound healing on day 7 (Figure S14A, Supporting Information). The diabetic wounds treated with TE-CM-4 and TE-CM-4+NIR possessed both significantly thinner granulation tissues on days 14 and 21 (Figure 7E,F) and relatively thicker epidermis layers on day 21 (Figure 7E,G) comparing to that of the control and 3 M groups, but the regenerated tissues of the adhesive groups were obviously denser, thus can better serve as a physical barrier like normal skin, to protect against infectious agents and mechanical injury. In the case of acute wound healing, the administration of TE-CM-4 or TE-CM-4+NIR also induced significantly increased granulation tissue thickness and collagen deposition comparing to that of the control and 3 M groups (Figure S14A–C, Supporting Information). On the 21st day, the wounds of the four groups all completely healed, but the scar areas of the TE-CM-4 and TE-CM-4+NIR groups were much smaller than that of the other two groups, which can also be proved by that more skin appendages including hair follicles, sebaceous glands, and squamous epithelium were found in the adhesive groups (Figure 7E and Figure S13, Supporting Information). These results preliminarily proved that the administration of TE-CMBAs could effectively accelerate diabetic wound healing through the promotion of re-epithelialization, regulation of granulation tissue formation and regeneration of skin appendages.

2.8.2. Microenvironment Modulation and Angiogenesis Promotion Effect of TE-CMBAs to Accelerate Diabetic Wound Healing

Oxidative stress can activate multiple signaling pathways, resulting in the overexpression of chemokines and inflammatory cytokines, and upregulated inflammatory reaction, which is believed to be the main reason for prolonged healing time or even nonhealing of diabetic wounds.[4,69,72] As a typical inflammatory cytokine, IL-1β closely relates to the inflammatory response in the early healing stage.[2,4] As shown in the IL-1β immunohistochemical stained images in **Figure 8**A, the highest IL-1β expression of the control group appeared on day 14 (Figure 8B), further confirming the prolonged healing time of diabetic wounds comparing to that of acute wounds, in which acute inflammatory reaction occurred in the first week (Figure S15A, Supporting Information). On day 7, the diabetic wounds were still mostly covered with necrotic adipose tissue, and the recruitment of inflammatory cells was hindered, leading to a lower IL-1β expression level than that of day 14, especially for the control and 3 M groups (Figure 8A,B). The IL-1β expression levels of the TE-CM-4 group on day 7 ($p < 0.05$), 14 ($p < 0.01$), and 21 ($p < 0.01$) were all significantly lower than that of the control and 3 M groups, and the inclusion of NIR irradiation group further reduced the IL-1β expression levels (Figure 8B). In addition, the IL-1β expression levels of adhesive groups continuously decreased along with time extension (Figure 8B), with the same trend as the acute wound healing case (Figure S15B, Supporting Information), indicating that TE-CM-4 (with or without NIR) can provide effective anti-inflammatory function. The excellent anti-oxidant activity enabled TE-CMBA with ROS scavenging capability, and NIR irradiation further switched on the photothermal antimicrobial activity of TE-CMBA to effectively eliminate bacterial infection and provide thermal stimulation beneficial for wound healing, which together downregulate the inflammatory reaction and accelerates the transition of diabetic wound healing from inflammatory phase to proliferative phase.

Neovascularization is a key factor reflecting the degree of skin tissue regeneration and function restoration, enhancing neovascularization can promote dermis regeneration and intact skin formation.[73] As shown in Figure 8C,D, for all groups, the amounts of CD31 positive cells increased from day 7 to day 14, then decreased. And the numbers of CD31 positive cells in the TE-CM-4 and TE-CM-4+NIR groups were significantly larger

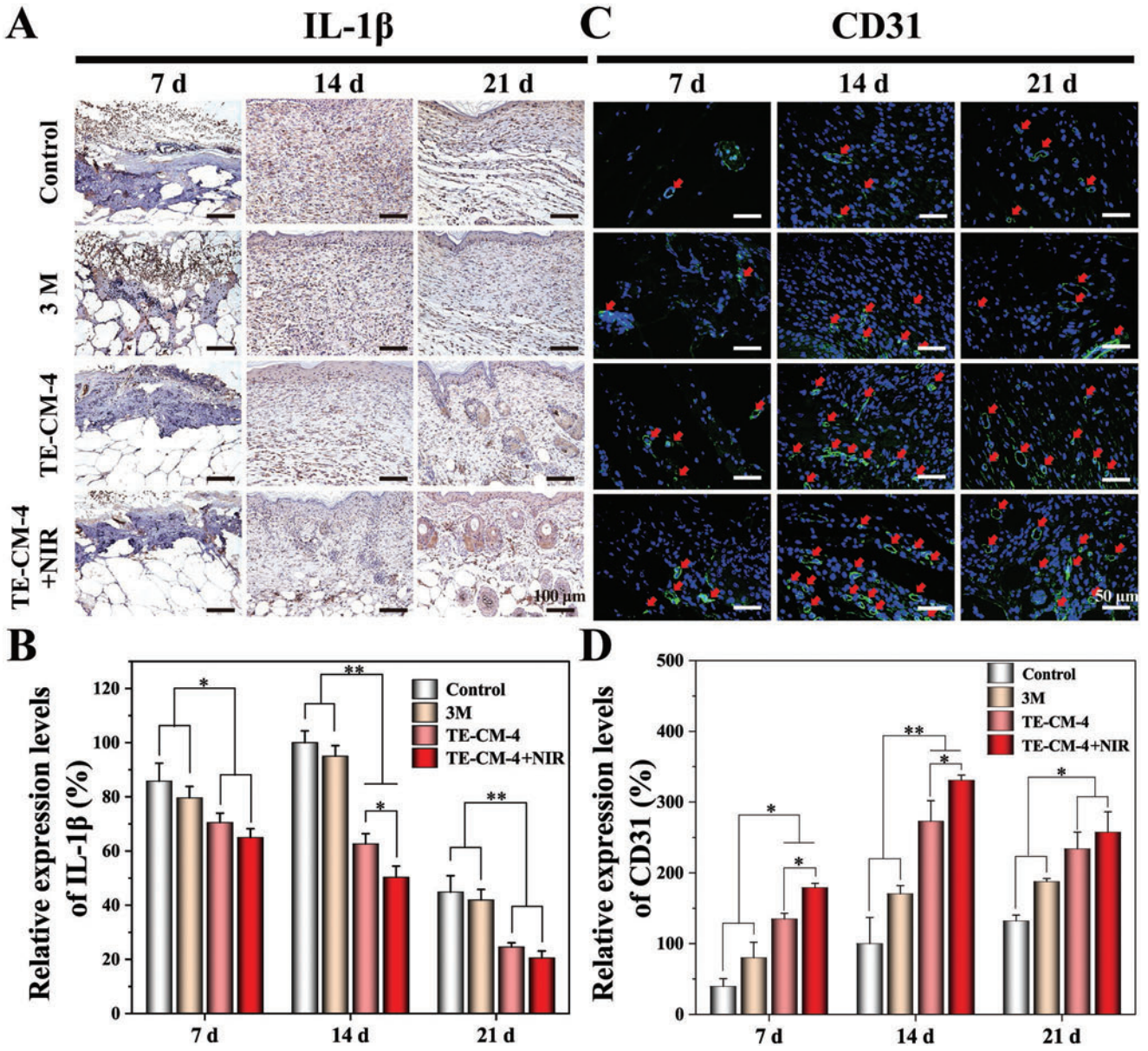

Figure 8. Inflammation and angiogenesis related immunohistochemical/immunofluorescence analysis: A) representative immunohistochemical staining images and B) quantitative analysis of the relative expression levels of IL-1β on day 7, 14, and 21 ($n = 3$); C) representative immunofluorescence staining images and D) quantitative analysis of the relative expression levels of CD31 on day 7, 14, and 21 ($n = 3$). For all quantitative data, the value of the control group on day 14 was set as 100%. *$p < 0.05$, **$p < 0.01$.

than that of the control and 3 M groups at all the three tested time-points, exhibiting a trend as the case of acute wound healing (Figure S15C,D Supporting Information), further confirming the excellent angiogenetic activity of TE-CMBAs derived from Eu^{3+} and TA. The favorable acid-induced fast Eu^{3+} and TA releasing properties in the diabetic wound sites also served as another factor to enhance TE-CMBAs' angiogenetic activity. Enhanced neovascularization facilitates the transport of nutrients, oxygen, and macrophages, to support cell proliferation and tissue reconstruction during diabetic wound healing.

ECM production, usually reflected as collagen deposition, and matrix degradation are in a dynamic balance in normal tissues to maintain their functions.[74,75] Due in part to the overexpression of ECM proteinases and their imbalance with inhibitors in diabetic wound bed, the ECM accumulation is dramatically reduced, impeding epithelial closure and prolonging diabetic wound healing.[27,76] Thus the effect of TE-CMBAs with/without NIR irradiation to the collagen deposition and the activity of matrix degradation was investigated using Masson's trichrome staining as well as collagen I (COL I) and metalloproteinase-2 (MMP2) immunohistochemical staining. From **Figure 9**A, it can be seen that on day 7, the diabetic wounds were mostly covered with adipose tissue, only the treated tissue of the TE-CM-4+NIR group had a thin epithelial layer stained in blue color (collagen), consistent with the H&E staining images shown in Figure 7E. More and denser collagen deposition can be found

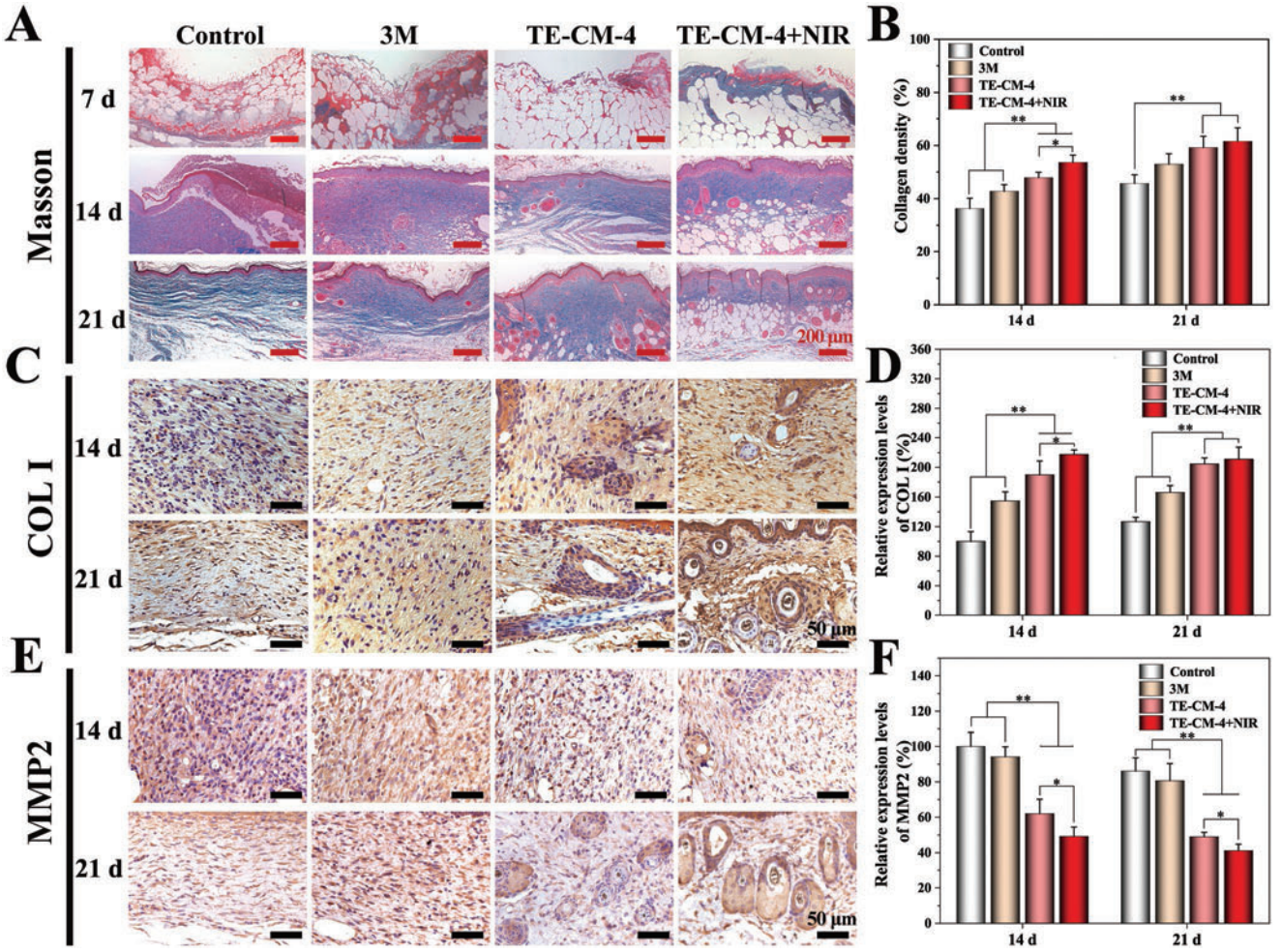

Figure 9. Analysis of collagen deposition and MMP2 activity: A) representative Masson's trichrome staining images and B) the calculated collagen densities on days 7, 14, and 21 ($n = 5$); C) immunohistochemical staining images and D) relative expression levels of collagen I on day 14 and 21 ($n = 4$); E) representative immunohistochemical staining images and F) relative expression levels of MMP2 on day 14 and 21 ($n = 4$). *$p < 0.05$, **$p < 0.01$.

in the two adhesive groups on day 14 and 21 (Figure 9A), the quantitative collagen densities of these two groups were significantly higher ($p < 0.01$) than that of the control and 3 M groups (Figure 9B), indicating that the application of TE-CMBAs with/without NIR irradiation could enhance collagen deposition in the process of diabetic wound healing. COL I is one of the main collagen types in the ECM of dermis. The immunohistochemical staining specially on COL I (Figure 9C,D) further confirmed the same trend that the administration of TE-CMBA (especially plus NIR) induced more collagen deposition.

Metalloproteinases (MMPs) are ECM degrading proteins playing important roles in all stages of wound healing, thus can serve as potential predictors of impaired healing in diabetic wounds. As shown in Figure 9E,F, the MMP2 expression levels of TE-CM-4 and TE-CM-4+NIR groups were significantly ($p < 0.01$) than the control and 3 M groups on day 14 and 21. The high expression level of IL-1β in diabetic wound tissue might induce the phosphorylation of p38 phosphorylation, which activates the p38 mitogen-activated protein kinase (MAPK) pathway and triggers the secretion of MMPs, resulting in the degradation of ECM and impaired wound healing.[75] The administration of anti-oxidant TE-CMBAs provided excellent anti-inflammatory efficacy to suppress the expression of pro-inflammatory cytokines like IL-1β, thus downgraded the expression of MMPs, further enhanced effective extracellular matrix deposition to accelerate diabetic wound healing.

3. Conclusions

In summary, ingeniously utilizing the multifaceted bonding ability of naturally derived anti-oxidant TA to both metal ions and hydrogen bond donors/acceptors containing polymers, a family of TE-CMBAs were specially developed for diabetic wound healing, via a simple physical mixing of TEC with iCMBA prepolymers. The obtained TE-CMBAs gelled instantly, possessed shape-adaptability, low swelling ratios, high elasticity, considerable wet tissue adhesiveness, favorable photothermal antimicrobial activity, good biocompatibility, as well as excellent anti-oxidant activity and angiogenetic property derived from both TA and Eu^{3+}. Most importantly, benefiting from the reversible hydrogen bond crosslinking between TEC and iCMBA prepolymers and the sensitive metal–phenolic coordination in TEC, TE-CMBAs also exhibited fast self-healability, tunable degradability, pH-responsive Eu^{3+} and TA releasing properties

and on-demand dissolvability/removability upon mixing with a mild sodium tetraborate pentahydrate (borax) solution. The in vivo wound healing experiments on diabetic db/db mice further confirmed that TE-CMBAs (with/without NIR) can modulate the inflammatory microenvironment by significantly downregulating the expression of pro-inflammatory cytokines, promote angiogenesis, and enhance ECM production and re-epithelialization by synchronously enhancing collagen deposition and decreasing the activities of MMPs. Overall, by providing drug-free anti-infection capability, alleviating oxidative stress, reducing inflammatory reactions, promoting angiogenesis and inhibiting matrix degradation, TE-CMBAs facilitate the smooth transition from the inflammatory to proliferation stages, in which wound closure, re-epithelialization, granulation tissue synthesis, extracellular matrix deposition, and tissue remodeling would sequentially occur, providing a potential comprehensive strategy to address the challenge of diabetic wound healing. TE-CMBAs also have great application potential in other complicated wound/tissue healing scenarios with the conditions of physiological dysfunction, high bacterial infection risk, and poor internal and external microenvironment, and the design principles of TE-CMBAs can also be universally expanded to inspire the development of smart therapeutic tissue adhesives.

Supporting Information

Supporting Information is available from the Wiley Online Library or from the author.

Acknowledgements

M.F. and Y.Z. contributed equally to this work. This work was supported by the Natural Science Foundation of China (Grant Nos. 82272453, U21A2099, 82102545, and 32201077), the Chinese Post-doctoral Science Foundation (Grant No. 2021M701627), and the Guangdong Basic and Applied Basic Research Foundation (Grant Nos. 2022A1515011982 and 2020A1515110062). All animal experiments were conducted in compliance with the Animal Experimental Committee of Institute of Biological and Medical Engineering, Guangdong Academy of Sciences (Approval No.2021011).

Conflict of Interest

The authors declare no conflict of interest.

Data Availability Statement

The data that support the findings of this study are available from the corresponding author upon reasonable request.

Keywords

diabetic wound healing, europium, on-demand removal, pH-responsive releasing, tannin

Received: September 5, 2022
Revised: October 8, 2022
Published online:

[1] H. Sun, P. Saeedi, S. Karuranga, M. Pinkepank, K. Ogurtsova, B. B. Duncan, C. Stein, A. Basit, J. C. N. Chan, J. C. Mbanya, M. E. Pavkov, A. Ramachandaran, S. H. Wild, S. James, W. H. Herman, P. Zhang, C. Bommer, S. Kuo, E. J. Boyko, D. J. Magliano, *Diabetes Res. Clin. Pract.* **2022**, *183*, 109119.
[2] H. Chen, Y. Cheng, J. Tian, P. Yang, X. Zhang, Y. Chen, Y. Hu, J. Wu, *Sci. Adv.* **2020**, *6*, eaba4311.
[3] K. Alexiadou, J. Doupis, *Diabetes Ther.* **2012**, *3*, 4;
[4] Y. Guan, H. Niu, Z. Liu, Y. Dang, J. Shen, M. Zayed, L. Ma, J. Guan, *Sci. Adv.* **2021**, *7*, eabj0153.
[5] W. Li, L. Jiang, S. Wu, S. Yang, L. Ren, B. Cheng, J. Xia, *Small* **2022**, *18*, e2107544.
[6] X. Ding, G. Li, P. Zhang, E. Jin, C. Xiao, X. Chen, *Adv. Funct. Mater.* **2021**, *31*, 2011230.
[7] L. Pang, P. Tian, X. Cui, X. Wu, X. Zhao, H. Wang, D. Wang, H. Pan, *ACS Appl. Mater. Interfaces* **2021**, *13*, 29363.
[8] Y. Qian, Y. Zheng, J. Jin, X. Wu, K. Xu, M. Dai, Q. Niu, H. Zheng, X. He, J. Shen, *Adv. Mater.* **2022**, *34*, 2200521.
[9] M. Wu, Z. Lu, K. Wu, C. Nam, L. Zhang, J. Guo, *J. Mater. Chem. B* **2021**, *9*, 7063.
[10] B. Chen, H. Zhang, J. Qiu, S. Wang, L. Ouyang, Y. Qiao, X. Liu, *Small* **2022**, *18*, e2201766.
[11] J. Mao, L. Chen, Z. Cai, S. Qian, Z. Liu, B. Zhao, Y. Zhang, X. Sun, W. Cui, *Adv. Funct. Mater.* **2022**, *32*, 2111003.
[12] L. J. Pruett, C. H. Jenkins, N. S. Singh, K. J. Catallo, D. R. Griffin, *Adv. Funct. Mater.* **2021**, *31*, 2104337.
[13] M. Wang, C. Wang, M. Chen, Y. Xi, W. Cheng, C. Mao, T. Xu, X. Zhang, C. Lin, W. Gao, Y. Guo, B. Lei, *ACS Nano* **2019**, *13*, 10279.
[14] H. K. D. Saleh, R. Portillo-Lara, E. S. Sani, R. Abdi, M. M. Amiji, N. Annabi, *Small* **2019**, *15*, e1902232.
[15] H. Chen, R. Cheng, X. Zhao, Y. Zhang, A. Tam, Y. Yan, H. Shen, Y. S. Zhang, J. Qi, Y. Feng, L. Liu, G. Pan, W. Cui, L. Deng, *NPG Asia Mater.* **2019**, *11*, 3.
[16] Y. Lu, H. Li, J. Wang, M. Yao, Y. Peng, T. Liu, Z. Li, G. Luo, J. Deng, *Adv. Funct. Mater.* **2021**, *31*, 2105749.
[17] S. Liu, Q. Zhang, J. Yu, N. Shao, H. Lu, J. Guo, X. Qiu, D. Zhou, Y. Huang, *Adv. Healthcare Mater.* **2020**, *9*, 2000198.
[18] P. Patil, K. A. Russo, J. T. McCune, A. C. Pollins, M. A. Cottam, B. R. Dollinger, C. R. DeJulius, M. K. Gupta, R. D'Arcy, J. M. Colazo, F. Yu, M. G. Bezold, J. R. Martin, N. L. Cardwell, J. M. Davidson, C. M. Thompson, A. Barbul, A. H. Hasty, S. A. Guelcher, C. L. Duvall, *Sci. Transl. Med.* **2022**, *14*, eabm6586.
[19] J. Liu, M. Qu, C. Wang, Y. Xue, H. Huang, Q. Chen, W. Sun, X. Zhou, G. Xu, X. Jiang, *Small* **2022**, *18*, 2106172.
[20] Z. Tu, M. Chen, M. Wang, Z. Shao, X. Jiang, K. Wang, Z. Yao, S. Yang, X. Zhang, W. Gao, C. Lin, B. Lei, C. Mao, *Adv. Funct. Mater.* **2021**, *31*, 2100924.
[21] S. A. Castleberry, B. D. Almquist, W. Li, T. Reis, J. Chow, S. Mayner, P. T. Hammond, *Adv. Mater.* **2016**, *28*, 1809.
[22] W. Srifa, N. Kosaric, A. Amorin, O. Jadi, Y. Park, S. Mantri, J. Camarena, G. C. Gurtner, M. Porteus, *Nat. Commun.* **2020**, *11*, 2470.
[23] F. Bao, G. Pei, Z. Wu, H. Zhuang, Z. Zhang, Z. Huan, C. Wu, J. Chang, *Adv. Funct. Mater.* **2020**, *30*, 2005422.
[24] M. Hosseini, A. Shafiee, *Small* **2021**, *17*, e2101384.
[25] T. Su, M. Zhang, Q. Zeng, W. Pan, Y. Huang, Y. Qian, W. Dong, X. Qi, J. Shen, *Bioact. Mater.* **2021**, *6*, 579.
[26] X. Zhao, D. Pei, Y. Yang, K. Xu, J. Yu, Y. Zhang, Q. Zhang, G. He, Y. Zhang, A. Li, Y. Cheng, X. Chen, *Adv. Funct. Mater.* **2021**, *31*, 2009442.
[27] Y. Liang, M. Li, Y. Yang, L. Qiao, H. Xu, B. Guo, *ACS Nano* **2022**, *16*, 3194.
[28] B. R. Freedman, O. Uzun, N. M. M. Luna, A. Rock, C. Clifford, E. Stoler, G. Ostlund-Sholars, C. Johnson, D. J. Mooney, *Adv. Mater.* **2021**, *33*, 2008553.

[29] K. Wu, M. Fu, Y. Zhao, E. Gerhard, Y. Li, J. Yang, J. Guo, *Bioact. Mater.* **2023**, *20*, 93.
[30] Z. Qiao, X. Lv, S. He, S. Bai, X. Liu, L. Hou, J. He, D. Tong, R. Ruan, J. Zhang, J. Ding, H. Yang, *Bioact. Mater.* **2021**, *6*, 2829.
[31] Y. Liang, X. Zhao, T. Hu, B. Chen, Z. Yin, P. X. Ma, B. Guo, *Small* **2019**, *15*, 1900046.
[32] J. Zhang, Y. Zheng, J. Lee, J. Hua, S. Li, A. Panchamukhi, J. Yue, X. Gou, Z. Xia, L. Zhu, X. Wu, *Nat. Commun.* **2021**, *12*, 1670.
[33] X. Zhao, Y. Liang, Y. Huang, J. He, Y. Han, B. Guo, *Adv. Funct. Mater.* **2020**, *30*, 1910748.
[34] K. Zhou, D. Chigan, L. Xu, C. Liu, R. Ding, G. Li, Z. Zhang, D. Pei, A. Li, B. Guo, X. Yan, G. He, *Small* **2021**, *17*, 2101858.
[35] T. Xie, J. Ding, X. Han, H. Jia, Y. Yang, S. Liang, W. Wang, W. Liu, W. Wang, *Mater. Horiz.* **2020**, *7*, 605.
[36] J. Cao, P. Wu, Q. Cheng, C. He, Y. Chen, J. Zhou, *ACS Appl. Mater. Interfaces* **2021**, *13*, 24095.
[37] X. Qi, Y. Xiang, E. Cai, S. You, T. Gao, Y. Lan, H. Deng, Z. Li, R. Hu, J. Shen, *Chem. Eng. J.* **2022**, *439*, 135691.
[38] A. Bal-Ozturk, B. Cecen, M. Avci-Adali, S. N. Topkaya, E. Alarcin, G. Yasayan, Y.-C. E. Li, B. Bulkurcuoglu, A. Akpek, H. Avci, K. Shi, S. R. Shin, S. Hassan, *Nano Today* **2021**, *36*, 101049;
[39] Y. Li, J. Cheng, P. Delparastan, H. Wang, S. J. Sigg, K. G. DeFrates, Y. Cao, P. B. Messersmith, *Nat. Commun.* **2020**, *11*, 3895.
[40] J. Guo, W. Sun, J. P. Kim, X. Lu, Q. Li, M. Lin, O. Mrowczynski, E. B. Rizk, J. Cheng, G. Qian, J. Yang, *Acta Biomater.* **2018**, *72*, 35.
[41] C. Cui, W. Liu, *Prog. Polym. Sci.* **2021**, *116*, 101388.
[42] C. Ma, E. Gerhard, D. Lu, J. Yang, *Biomaterials* **2018**, *178*, 383.
[43] X. Lu, S. Shi, H. Li, E. Gerhard, Z. Lu, X. Tan, W. Li, K. M. Rahn, D. Xie, G. Xu, F. Zou, X. Bai, J. Guo, J. Yang, *Biomaterials* **2020**, *232*, 119719;
[44] X. Yuan, Y. Zhao, J. Li, X. Chen, Z. Lu, L. Li, J. Guo, *J. Mater. Chem. B* **2021**, *9*, 8202.
[45] W. Zhang, R. Wang, Z. Sun, X. Zhu, Q. Zhao, T. Zhang, A. Cholewinski, F. Yang, B. Zhao, R. Pinnaratip, P. K. Forooshani, B. P. Lee, *Chem. Soc. Rev.* **2020**, *49*, 433.
[46] L. Zhou, J. Ge, M. Wang, M. Chen, W. Cheng, W. Ji, B. Lei, *Bioact. Mater.* **2021**, *6*, 1605.
[47] J.-X. Fan, D.-W. Zheng, W.-W. Mei, S. Chen, S.-Y. Chen, S.-X. Cheng, X.-Z. Zhang, *Small* **2017**, *13*, 1702714.
[48] C. Zhang, B. Wu, Y. Zhou, F. Zhou, W. Liu, Z. Wang, *Chem. Soc. Rev.* **2020**, *49*, 3605.
[49] X. Qi, Y. Huang, S. You, Y. Xiang, E. Cai, R. Mao, W. Pan, X. Tong, W. Dong, F. Ye, J. Shen, *Adv. Sci.* **2022**, *9*, e2106015.
[50] K. Kim, M. Shin, M.-Y. Koh, J. H. Ryu, M. S. Lee, S. Hong, H. Lee, *Adv. Funct. Mater.* **2015**, *25*, 2402.
[51] Y.-N. Chen, L. Peng, T. Liu, Y. Wang, S. Shi, H. Wang, *ACS Appl. Mater. Interfaces* **2016**, *8*, 27199.
[52] S. Bai, X. Zhang, X. Lv, M. Zhang, X. Huang, Y. Shi, C. Lu, J. Song, H. Yang, *Adv. Funct. Mater.* **2020**, *30*, 1908381.
[53] Y. Guo, Q. Sun, F.-G. Wu, Y. Dai, X. Chen, *Adv. Mater.* **2021**, *33*, 2007356;
[54] K. Wu, X. Wu, J. Guo, Y. Jiao, C. Zhou, *Adv. Healthcare Mater.* **2021**, *10*, 2100793.
[55] Y. Feng, P. Li, J. Wei, *Coord. Chem. Rev.* **2022**, *468*, 214649.
[56] Y. Li, Y. Miao, L. Yang, Y. Zhao, K. Wu, Z. Lu, Z. Hu, J. Guo, *Adv. Sci.* **2022**, *9*, 2202684.
[57] M. Shi, L. Xia, Z. Chen, F. Lv, H. Zhu, F. Wei, S. Han, J. Chang, Y. Xiao, C. Wu, *Biomaterials* **2017**, *144*, 176.
[58] C. R. Patra, R. Bhattacharya, S. Patra, N. E. Vlahakis, A. Gabashvili, Y. Koltypin, A. Gedanken, P. Mukherjee, D. Mukhopadhyay, *Adv. Mater.* **2008**, *20*, 753.
[59] J. Wei, G. Wang, F. Chen, M. Bai, Y. Liang, H. Wang, D. Zhao, Y. Zhao, *Angew. Chem., Int. Ed.* **2018**, *57*, 9838.
[60] J. Wang, X.-Y. Chen, Y. Zhao, Y. Yang, W. Wang, C. Wu, B. Yang, Z. Zhang, L. Zhang, Y. Liu, X. Du, W. Li, L. Qiu, P. Jiang, X.-Z. Mou, Y.-Q. Li, *ACS Nano* **2019**, *13*, 11686.
[61] Y. Yang, X. Zhao, J. Yu, X. Chen, R. Wang, M. Zhang, Q. Zhang, Y. Zhang, S. Wang, Y. Cheng, *Bioact. Mater.* **2021**, *6*, 3962.
[62] F. Sun, Y. Bu, Y. Chen, F. Yang, J. Yu, D. Wu, *ACS Appl. Mater. Interfaces* **2020**, *12*, 9132.
[63] J. Qu, X. Zhao, Y. Liang, T. Zhang, P. X. Ma, B. Guo, *Biomaterials* **2018**, *183*, 185.
[64] Y. Liang, Z. Li, Y. Huang, R. Yu, B. Guo, *ACS Nano* **2021**, *15*, 7078.
[65] L. Zhao, L. Niu, H. Liang, H. Tan, C. Liu, F. Zhu, *ACS Appl. Mater. Interfaces* **2017**, *9*, 37563.
[66] Z. Bei, Y. Lei, R. Lv, Y. Huang, Y. Chen, C. Zhu, S. Cai, D. Zhao, Q. You, Y. Cao, X. Zhang, *ACS Nano* **2020**, *14*, 12546.
[67] X. Tan, E. Gerhard, Y. Wang, R. T. Tran, H. Xu, S. Yan, E. B. Rizk, A. D. Armstrong, Y. Zhou, J. Du, X. Bai, J. Yang, *Small* **2022**, *18*, 2203003.
[68] T. Wang, Y. Li, E. J. Cornel, C. Li, J. Du, *ACS Nano* **2021**, *15*, 9027.
[69] H. Zhao, J. Huang, Y. Li, X. Lv, H. Zhou, H. Wang, Y. Xu, C. Wang, J. Wang, Z. Liu, *Biomaterials* **2020**, *258*, 120286.
[70] V. S. Bollu, S. K. Nethi, R. K. Dasari, S. S. Rao, S. Misra, C. R. Patra, *Nanotoxicology* **2016**, *10*, 413.
[71] G. H. Tesch, A. K. Lim, *Am. J. Physiol. Renal. Physiol.* **2011**, *300*, F301.
[72] A. E. Boniakowski, A. S. Kimball, B. N. Jacobs, S. L. Kunkel, K. A. Gallagher, *J. Immunol.* **2017**, *199*, 17.
[73] Y. Yuan, S. Shen, D. Fan, *Biomaterials* **2021**, *276*, 120838.
[74] L. Liu, Z. Ding, Y. Yang, Z. Zhang, Q. Lu, D. L. Kaplan, *Biomater. Sci.* **2021**, *9*, 5227.
[75] J. Dai, J. Shen, Y. Chai, H. Chen, *Mediators Inflammation* **2021**, *2021*, 6645766.
[76] J. Sonamuthu, Y. Cai, H. Liu, M. S. M. Kasim, V. R. Vasanthakumar, B. Pandi, H. Wang, J. Yao, *Int. J. Biol. Macromol.* **2020**, *153*, 1058.

NANO MICRO small

Supporting Information

for *Small,* DOI: 10.1002/smll.202205489

On-Demand Removable Self-Healing and pH-Responsive Europium-Releasing Adhesive Dressing Enables Inflammatory Microenvironment Modulation and Angiogenesis for Diabetic Wound Healing

Meimei Fu, Yitao Zhao, Yue Wang, Yue Li, Min Wu, Qi Liu, Zhiguo Hou, Zhihui Lu, Keke Wu, and Jinshan Guo**

Supporting Information

On-demand removable self-healing and pH-responsive europium-releasing adhesive dressing enables inflammatory microenvironment modulation and angiogenesis for diabetic wound healing

Meimei Fu[#], Yitao Zhao[#], Yue Wang, Yue Li, Min Wu, Qi Liu, Zhiguo Hou, Zhihui Lu, Keke Wu* and Jinshan Guo*

M. Fu, Y. Zhao, Y. Wang, Y. Li, M. Wu, Prof. Z. Lu, Prof. K. Wu, Prof. J. Guo,
Department of Histology and Embryology, School of Basic Medical Sciences, Guangdong Provincial Key Laboratory of Bone and Joint Degeneration Diseases, The Third Affiliated Hospital of Southern Medical University, Southern Medical University, Guangzhou, 510515, P. R. China

Q. Liu, Z. Hou, Prof. Z. Lu
Regenerative Medicine and Tissue Repair Material Research Center, Huangpu Institute of Materials, Guangzhou, 510530, P. R. China

Y. Li

Department of Plastic and Aesthetic Surgery, Nanfang Hospital of Southern Medical University, Guangzhou, 510515, P. R. China

*Corresponding Emails: jsguo4127@smu.edu.cn (J. Guo, Tel: +86-20-61648222); kkwu@smu.edu.cn (K. Wu).
[#]These authors contribute equally.

Keywords: tannin, europium, diabetic wound healing, on-demand removal, pH-responsive releasing

Experimental Section

Materials

Citric acid, poly (ethylene glycol)-block-poly (propylene glycol)-block-poly (ethylene glycol) (PEG-PPG-PEG, EPE, M_n = 1100 Da) and dopamine hydrochloride (DP) were purchased from Sigma-Aldrich. Tannic acid (TA), $Eu(NO_3)_3.6H_2O$ were purchased from Macklin Reagent. Calcium carbonate ($CaCO_3$), sodium tetraborate pentahydrate (borax) and ethanol were purchased from Aladdin Biological Technology Co., Ltd (Shanghai, China). All chemicals were analytical reagents and used as received.

Synthesis of TEC coordination complex

An alkaline TA solution was obtained by adding ammonia aqueous solution (100 μL, 25 wt%) into TA (0.5 g) solution in deionized water (30 mL) under stirring. Then, $Eu(NO_3)_3.6H_2O$ (0.5

g) in deionized water (10 mL) was added dropwise to the alkaline TA solution to give a flocculent precipitation. After stirring for 10 min, the reaction mixture was centrifuged at 5000 rpm for 10 min, washed with deionized water 3 times, and then freeze-dried for 24 hours to obtain tannin-europium coordination complex (TEC). The morphology of TEC was observed by scanning electron microscopy (SEM, Quanta 200, Japan) and the particle size analysis was also conducted by measuring the sizes of at leat 300 particles and averaged. the crystallinity and element compositions of TEC were also characterized by X-ray diffraction (XRD, Bruker D8) and X-ray photoelectron spectroscopy (XPS, Thermo Fisher Scientific, Escalab 250Xi) respectively. The Fourier transform infrared (FTIR) spectrum of TEC was also recorded by an infrared spectrometer (Thermo Scientific, Nicolet-iS10).

Synthesis of $CaCO_3$ treated EPE containing iCMBA (iC-E-Ca^{2+}) prepolymer

The iC-E-Ca^{2+} prepolymer was synthesized adapted from our previous work[1]. Briefly, a mixture of CA (11.528 g), EPE (55 g), and dopamine hydrochloride (2.844 g) was heated to 160 °C in a round-bottomed flask under stirring until melting. The melted mixture was then reacted at 140 °C until the stirrer cannot rotate. The temperature was reduced and ethanol was added to dissolve the obtained prepolymer, and then excess $CaCO_3$ (21 g) was added and the mixture was stirred overnight. After that, the reaction mixture was dialyzed against deionized water using a dialysis tube (with a molecular weight cut-off (MWCO) of 1000 Da) for 3 days, the residual $CaCO_3$ solid was removed by centrifugation, and the remaining solution was freeze-dried to give purified water soluble iC-E-Ca^{2+} prepolymer.

Gelation and physical properties of TE-CMBAs

The iC-E-Ca^{2+} prepolymer was dissolved in water to form a 33 wt% solution, and TEC powder was dispersed in deionized water to prepare a 15 wt% dispension solution. Then the iC-E-Ca^{2+} solution and TEC dispersion solution were mixed at room temperature (25 °C) in volume ratios of 20: 1, 20: 2, 20: 4, and 20: 10, the obtained adhesives were named as TE-CM-1, TE-CM-2, TE-CM-4 and TE-CM-10 respectively (Table S1). The adhesives crosslinked at 37 °C were also prepared for comparison. The FTIR spectra of iC-E-Ca^{2+} and representative TE-CMBAs were recorded with an infrared spectrometer.

The gel times of the adhesives were obtained by the tilting test method according to previous literature [1]. The timing began with the two solutions being uniformly mixed, and stopped with a precipitate formation. A total of five duplicates were set for each sample and the results were averaged.

The sol contents of TE-CMBAs of different formulations were measured by the mass change before and after incubation of the dried crosslinked adhesive hydrogels in 1, 4-dioxane to

remove the soluble part. Briefly, the dried adhesive were die-cut into a circular sheet with a diameter of 5 mm and a thickness of 1.5 mm, and the initial mass (W_i) was recorded. Then it was immersed in 1, 4-dioxane for 48 hours and the solvent was changed every 6 hours. Finally, the adhesive was freeze-dried and weighed (W_d). The sol content was calculated using Equation (1).

$$\text{Sol content (\%)} = \frac{W_i - W_d}{W_i} \times 100\% \quad (1)$$

The swelling ratios of TE-CMBAs were measured by the mass difference of the dried TE-CMBA adhesives (removed the sol part, W_d) before and after being immersed in water until a swelling equilibrium (W_s) was reached. The swelling ratio was calculated using Equation (2).

$$\text{Swelling ratio (\%)} = \frac{W_s - W_d}{W_d} \times 100\% \quad (2)$$

Mechanical properties of TE-CMBAs

The mechanical property of TE-CMBAs was measured using an Instron 34TM-10 testing machine with a 500 N load cell according to American Society for Testing and Materials (ASTM) standard D412A. The TE-CMBAs with different formulations were cast in Teflon molds and dried for three days to prepare dumbbell specimens (25 mm × 6 mm × 1.5 mm, length × width × thickness), which were stretched to failure at a strain rate of 500 mm min^{-1}. The initial modulus was calculated from the initial slope of the curve (0-10% elongation), tensile stress and elongation at break were also measured from the stress-strain curve for each specimen.Meanwhile, the mechanical properties of TE-CMBAs at wet state (using a 10 N load cell) was also investigated using the completely swollen specimens after the dried specimens being hydrated in water.

Adhesion strengths of TE-CMBAs

First, the universal adhesion of TE-CMBAs to various substrates including wood, plastic, rubber, glass, steel and fresh organs (heart, liver, spleen, lung and kidney) of Sprague-Dawley (SD) rat was testified and demonstrated in Figure 2C. The adhesion strengths of TE-CMBAs to wet tissue were also measured by lap-shear strength test according to the modified ASTM F2255-05 method as described in previous literatures [1-4]. Briefly, porcine skin was soaked in 1 mol/L NaOH solution to remove the fat of the inner layer, washed with deionized water, and then cut into rectangle strips (length × width = 30 mm × 10 mm). iC-E-Ca^{2+} solution (10 μL) and corresponding volumes of TEC solution for different formulations were applied to the ends of two porcine skin slides respectively, and then they were overlapped with each other to create a lap shear joint with an overlap area of 10 × 10 mm^2, the TE-CMBA solution was

uniformly mixed and cured at 37 °C for 2 hours under a humidity of 50%. Finally, the adhesive substrate was stretched at a constant tensile rate of 5 mm/min using an universal tensile machine (Instron 34TM-10) equipped with a 10 N load cell. The adhesion strength was calculated by dividing the maximum load (force) by the overlapping contact area. For each sample, at least 5 specimens were tested and the values were averaged.

Degradation profiles and pH responsive Eu^{3+} & TA release properties of TE-CMBAs

The fast degradation profiles of TE-CMBAs were studied by measuring the mass losses at preset time-points of the dried adhesive die-cut into circular plates (5 mm in diameter, 1.5 mm in thickness, the initial weight (W_i) was recorded) in NaOH (2 mol/L) at 37 °C, respectively. Moreover, A degradation of the dried TE-CMBA adhesives in phosphate-buffered salines (PBS, pH 7.4, 0.1 mol/L) was also conducted. The PBS solution was changed every the other day in the beginning and once a week later to ensure the degradation process. At the pre-set time points, the sample was collected, washed with deionized water, and freeze-dried to obtain the weight W_t. The mass loss was calculated using Equation (3). At least five parallels were set for each sample, and the results were averaged.

$$\text{Mass loss (\%)} = \frac{W_i - W_t}{W_i} \times 100\% \qquad (3)$$

The release of Eu^{3+} and tannic acid (TA) at different pH values (6, 7.4 and 8.5) was also studied by immersing the crosslinked dry TE-CMBA films in PBS solution (0.1 m) with different pH values at 37 °C, respectively. At pre-set time points (0.5, 1, 2, 3, 5, 7, 10, 14, 21 days), the Eu^{3+} concentrations were measured by ICP-MS (iCAP PRO, Thermo Fisher Scientific, MA, USA). At the same time, the concentration of released TA was determined by UV-vis spectrophotometer (Shimadzu, UV-2600).

Shape adaptability, self-healability ability and rheological testing of TE-CMBAs

The shape adaptability of TE-CMBAs was demonstrated by putting TE-CMBA (2 g)into a star mold, the mold filling situation of adhesive was observed at different time points and photographed.

To investigate the self-healability of TE-CMBAs, a piece of wet adhesive was cut into two parts and then the two parts were contacted with each other, and the fusion process was recorded by taking photos at different time points. In addition, the mechanical property of the healed adhesives was measured using an Instron 34TM-10 testing machine.

The self-healing behavior of TE-CMBA was further investigated by strain sweep tests (small strain γ = 1.0%, large strain γ = 100%) on a TA rheometer (DHR-2). The temperature was set at 37 °C, and the strain sweep tests were performed at an oscillatory frequency of 1 rad/s

while increasing strain from 0.01% to 100%. Small strain (0.01%) and large strain (100%) were scanned alternately for four cycles, and the changes of storage moduli and loss moduli were recorded.

On-demand removal property

Borax solution was found could dissolve the crosslinked TE-CMBAs, the dissolution behavior was testified both *in vitro* and *in vivo*. A certain amount of adhesive was charged to a sample bottle, then borax solutions with different concentrations were dropped in, and the dissolution behavior was observed, the dissolution time was also recorded. Furthermore, the full-thickness skin wounds were made, which were covered with a representative TE-CMBA, and then borax solution was applied, then the adhesive dissolution behavior was photographed. Moreover, oscillatory frequency scanning measurements were performed using a rheometer (DHR-2) at a strain of 10%, and a shear frequency of 0.1-10 rad/s at 25 °C, the storage moduli (G') and loss moduli (G") of the TE-CMBA before and after borax solution application was recorded.

Photothermal property and photothermal antibacterial activity of TE-CMBAs

To evaluate the photothermal response of TE-CMBAs, the adhesive samples were die-cut into uniform wafers, and then irradiated with 808 nm laser (B0T808-5W) with an energy density of 1 W/cm^2, and the temperature change was monitored and recorded by an infrared (NIR) thermal imaging system (UTI260B). TE-CM-4 was chosen as a representative adhesive to investigate the effect of power density change (0.8, 1.0, 1.2 W/cm^2) to the photothermal behavior. Four cycles of heating and cooling were also conducted to assess the repeatable photothermal properties of TE-CMBAs. The heat maps and temperature profiles of TE-CMBAs during light irradiation were recorded using an infrared (IR) thermal imaging camera (UTI165H). The results are shown in Figures 4A-4D. The *in vitro* antibacterial activities of TE-CMBAs with or without NIR irradiation was evaluated using *E. coli* (ATCC 8739) and *S. aureus* (ATCC 6538) as representative Gram-negative and Gram-positive bacteria. Briefly, a dried adhesive film (16 mm in diameter, 2 mm in thickness) was sterilized and added into 24-well plates. Then bacterial suspension (10 μL, ~1 × 10^8 colony-forming units (CFUs) /mL) was added onto the surface of the adhesive film and then exposed to NIR laser irradiation (808 nm, 1.0 W/cm^2) for 10 minutes. Untreated bacterial suspension was set as a negative control. After all samples were exposed to bacteria ± NIR irradiation for a preset time, sterile PBS (1 mL) was added to each well to re-suspend the surviving bacteria. Then, the diluted bacterial suspensions (100 μL) were uniformly casted on agar plates in petri

dishes and cultured at 37 °C for 12 hours followed by CFU counting. All experiments were performed in triplicate and the results were averaged.

***In vitro* anti-oxidant activity of TE-CMBAs**

The *in vitro* anti-oxidant activity of TE-CMBAs was assessed by both 2,2-diphenyl-1-picrylhydrazyl (DPPH) assay and cellular reactive oxygen species (ROS) assay. Briefly, freeze-dried TE-CMBA adhesive film (3 mg) was added into DPPH solution (4 mL, 100 μM) in methanol. After being incubated under dark for a preset time, the absorbance of the solution at 517 nm (A_s) was measured by a UV-vis spectrophotometer. The absorbance of the untreated DPPH solution (A_c) was used as the blank control. The DPPH scavenging percentage was calculated using Equation (4) [4].

$$\text{DPPH scavenging (\%)} = \frac{A_S - A_c}{A_c} \times 100\% \qquad (4)$$

The cellular ROS assay was also conducted. Briefly, mouse fibroblasts (L929) were seeded in both 96-well (for quantitative study) and 24-well (for microscopic observation) plates with a cell density of 8000 cells/cm^2 , the plates were incubated at 37°C for 12 hours. Then complete Dulbecco's modified Eagle's medium (DMEM, GIBCO, Themo Fisher scientific, with 10% (v/v) fetal bovine serum (FBS, Ausgenex, New Zealand, Australia) and 1% (v/v) penicillin/streptomycin (Cyagen Biosciences Inc. USA)) containing Rosup reagent (1 μg/mL) and 10× diluted TE-CMBA degradation product, prepared by degrading 1.0 g dried TE-CMBA in NaOH solution (10 mL, 1.0 M), neutralized, sterilized by passing through a 0.2 μm teflon filter and diluted 10 times with sterile PBS (pH 7.4), was added, and the cells were cultured for another 6 hours. After being washed twice with sterile PBS (pH 7.4), 2, 7-dichlorodihydrofluorescein diacetate (DCFH-DA) solution was added, and the mixture was incubated for 20 minutes. Then, the cells in 24-well plates were observed and photographed with an inverted fluorescent microscope (Olympus CKX41, Tokyo, Japan), and the cells in 96 well plates were quantitatively measured by a fluorescence microscope (Olympus CKX41, Tokyo, Japan). Cells treated with Rosup alone were used as the positive control, and cells without any treatment were used as the negative control.

***In vitro* cell experiments**

Cytocompatibility and cell proliferation evaluation

Mouse fibroblasts (L929) and human umbilical vein endothelial cells (HUVECs) were incubated in complete DMEM, with 10% (v/v) FBS and 1% (v/v) penicillin/streptomycin. Cells were cultured in a humidified incubator (Thermo Fisher Scientific, USA) at 37°C and 5% CO_2. DMEM medium was changed every the other day until the cells reached 80% confluence before use.

The cytocompatibility of Eu^{3+} and TEC was evaluated by cell Counting Kit-8 (CCK-8, Jiancheng Co, Nanjing, China) assay. Briefly, a certain amount of $Eu(NO_3)_3.6H_2O$ or TEC were directly dissovlved or dispersed in complete DMEM medium, sterilized under ultraviolet (UV) radiation for 2 hours and gradiently diluted to obtain a series of Eu^{3+} or TEC solutions. Then L929 cells were seeded in the wells of 96 well plates at a cell density of 4×10^4 cells/mL (100 μL/well), and incubated in complete DMEM medium for 12 hours. Then, Eu^{3+} and TEC solutions in complete DMEM with various dilutions was added and the cells were incubated for another day followed by CCK-8 assay according to the manufacturer's protocol. Cells cultured in pure DMEM were used as control. The cell viabilities was calculated by Equation (5). Ab_{sample} was the absorbance of the sample at 450 nm, and $Ab_{control}$ was the absorbance of the control at 450 nm.

$$\text{Cell viability (\%)} = Ab_{sample}/Ab_{control} \times 100\% \qquad (5)$$

The cytocompatibility of TE-CMBAs was evaluated using the sol contents and degradation products of TE-CMBAs by cell Counting Kit-8 assay against both L929 and HUVECs. For sol content, dried TE-CMBA (1.0 g) was incubated in PBS (10 mL, pH 7.4) at 37 °C for 24 hours, and the collected supernate was neutralized to pH 7.4, sterilized via filtration through a 0.2 μm filter, to obtain the 1× sol content. For degradation products, dried TE-CMBA (1.0 g) was fully degraded in NaOH solution (10 mL, 1.0 M) and the pH was adjusted to 7.4, the solution was further sterilized via filtration through a 0.2 μm filter to obtain the 1× degradation product. The concentration of sol contents and degradation products was then diluted 10 and 100 times, using PBS (pH 7.4), to obtain 10× and 100 × sol contents and degradation products respectively. L929 or HUVECs cells were seeded in 96 well plates. Then, sterilized sol content or degradation product (10 μL) with various dilutions was added and the cells were incubated for another day followed by CCK-8 assay according to the manufacturer's protocol. Cells cultured in pure DMEM were used as control. The cell viabilities was calculated by Equation (5). Ab_{sample} was the absorbance of the sample at 450 nm, and $Ab_{control}$ was the absorbance of the control at 450 nm.

Cell migration experiments

The effect of TE-CMBAs to the cell migration capability was evaluated by both scratch assay and transwell assay using 10 × degradation products. The detailed experimental processes are listed below.

For the scratch assay, L929 cells were seeded in 6-well plates with a cell density of ~5×10^5 cells/well. After being cultured in complete DMEM for 24 hours, a cell monolayer was formed, then three parallel scratches were created using a 200 μL pipette tip, the floating cells

was washed with sterile PBS (pH 7.4) for three times, and the remaining cells were cultured in complete DMEM containing 10× degradation products (1/10 to complete DMEM (v/v)) of different TE-CMBA formulations for one more day. 12 and 24 hours later, the cells were observed and photographed by an inverted microscope (Olympus CKX41, Tokyo, Japan), and the cell migration rate was quantitatively calculated by ImageJ and an analysis software, using the Equation (6).

$$\text{Migration rate (\%)} = \frac{W_i - W_t}{W_i} \times 100\% \qquad (6)$$

Here W_i denotes the initial scratch width at 0 h, W_t represents the scratch width after being cultured for t hours (t =12 or 24).

For the transwell assay, transwell chambers (Corning, 353097) were put into the wells of 24-well plates of the DMEM and 10 × degradation products and L929 cells with a density of 1×10^4 cells/mL were seeded in the chambers (500 μL/chamber) and cultured for 24 hours. Then the cells on the upper surface of the chamber were completely removed by wiping with a cotton swab, and the cells on the lower surface were subsequently fixed with 5% glutaraldehyde solution for 30 minutes and stained with crystal violet for 15 minutes, followed by washing with sterile PBS, being observed and photographed with an microscope (Olympus CKX41, Tokyo, Japan). Then the chamber was immersed in 30% glacial acetic acid for elution, and the OD value of the eluted solution at 570 nm was measured.

In vitro tube formation assay

The effect of TE-CMBAs to the vasculogenic ability of endothelial cells was evaluated by tan *in vitro* angiogenesis experiment using HUVECs. Matrigel matrix glue (100 μL, Corning, 356234) was added to each well of 48-well plates and gently shaken to cover the bottom of each well, and the plates were placed in a 37 °C incubator for more than 1 hour. Then HUVECs at a density of ~2×10^4 cells/mL in complete DMEM containing 10× degradation product were added to the matrix glue containing plate and incubated in at 37 °C, 5% CO_2 for 6 hours. The cell tube formation status was observed and photographed using an inverted microscope, and the average relative tube length was also quantitatively analyzed by ImageJ.

***In vivo* study**

Skin defect of C57BL/6 mice and type 2 diabetic db/db mice

The *in vivo* acute and chronic wound healing efficacy of TE-CMBAs were assessed using the full thickness wound models on wild mice (C57BL/6) and type 2 diabetic db/db (Leprdb/db) mice respectively. Male C57BL/6 mice (8 weeks, 30 ± 5g) and male db/db mice (8 weeks, 50 ± 5g) were purchased from the Experimental Animal Center of Southern Medical

University and Guangdong Yaokang Biotechnology Co., Ltd, respectively. All animal experiments were conducted in compliance with the Animal Experimental Committee of Institute of Biological and Medical Engineering, Guangdong Academy of Sciences (Approval No.2021011). The experimental animals were randomly divided into four groups (n = 5): control group, 3M (Tegaderm TM, 3M Health Care, St. Paul, MN, USA) group, TE-CM-4 group and TE-CM-4+NIR group. All animals were anesthetized by intraperitoneal injection of chloral hydrate (0.3 mg/kg), then the back hair was shaved with an electric animal razor, and further removed with a hair removal cream to fully expose the surgical site. Then surgical scissors were used to create four full-thickness wounds (diameter ~ 6 mm) on the shaved back of each mouse. After removing the wound skin, TE-CM-4 adhesive (200 μL) or 3M films were applied to the wounds, sterile PBS (50 μL, pH 7.4) was added to the wound of the control group. The 3M dressing was directly affixed with a transparent film. For the TE-CM-4+NIR group, the wounds covered with TE-CM-4 adhesive dressing were further irradiated with 808 nm NIR for 10 minutes. Dressings were applied and changed every five to seven days depending on the condition of the wound. The wound healing process was closely monitored and recorded by taking wound photos at 0, 7, 14, 21 days after surgery, followed by Image J analysis.

Histology and immunohistochemistry analysis

For the wound models on wild mice on the 7^{th}, and 14^{th} day post operation, the wound tissues treated by different samples were harvested, and on the 7^{th}, 14^{th}, and 21^{st} day post operation of type 2 diabetic db/db mice, the wound tissues treated by different samples were harvested, whose all fixed with 4% polyformaldehyde overnight, gradiently dehydrated, embedded in paraffin, and finally cut into 4 μm slices. Then the embedded tissue slices were used for histological (hematoxylin-eosin (H & E) and Masson's trichrome staining), interleukin-1β (IL-1β, purchased from Servicebio, China) immunohistochemical and platelet endothelial cell adhesion molecule-1 (CD31, from Servicebio, China) immunofluorescence staining, observed and recorded under a positive fluorescence microscope (Leica DM4000 B, Wetzlar, Germany) to investigate the wound epidermal regeneration, collagen deposition, inflammation, and vascularization. For the wound tissue slices of the db/db mice model, an additional collagen I (COL I, from Servicebio, China) and matrix metallopeptidase 2 (MMP2, purchased from Servicebio, China) immunohistochemical staining was also conducted.

Statistical analysis

All the experimental data were statistically analyzed and expressed as mean ± standard deviation (SD), and the statistical difference was determined by t-test or one-way ANOVA.

All the data are considered to have significant differences only when $p < 0.05$. * and ** represent $p < 0.05$ and $p < 0.01$, respectively.

Results of C57BL/6 mice wound healing assessment

To better demonstrate the wound healing efficacy of TE-CMBAs and compare with diabetic wound healing, an acute full-thickness wound on C57BL/6 mice was created (Figures 7A and S12) and treated by TE-CM-4 with/without NIR irradiation. The representative wound healing images and the wound closure quantitative analysis results on the 0, 7^{th} and 14^{th} days are shown in Figures S12A-S12C. The wound contraction rates of the TE-CM-4 and TE-CM-4+NIR groups were significantly faster than that of the control and 3M groups (Figure S12). On day 14, the wounds of all four groups almost healed completely, but the scar areas of the two adhesive groups were smaller than that of the control and 3M groups. These results indicate that the administration of TE-CMBAs as wound dressing can accelerate wound healing and ameliorate the cosmetic appearance of the wounds.

As shown in the hematoxylin and eosin (H & E) staining images in Figure S14A, on day 7, severe inflammatory cell infiltration could be found in the control and 3M groups, but the adhesive groups showed minor inflammatory response, which is confirmed by that the IL-1β expression levels of the adhesives groups were significantly lower ($p < 0.01$) than that of the control and 3M groups on day 7 (Figures S15A and S15B). The inflammatory response greatly reduced on day 14 (Figures S14A, S15A and S15B), conformed to the characteristic of acute wound healing. On day 14, the wound sites of four groups were covered with a complete epidermis and granulation tissue (Figure S14A). The granulation tissue thicknesses of the wounds treated with TE-CM-4 (832 ± 75 μm) and TE-CM-4+NIR (954 ± 55 μm) were significantly larger than that of the control (366 ± 50 μm) and 3M (542 ± 72 μm) groups (Figures S14A and S14B). The thicknesses of the dermis layer also showed a similar trend as control < 3M < TE-CM-4 < TE-CM-4+NIR (Figure S14A). More capillaries could also be seen in the adhesive treated wounds (Figure S14A), which can also be confirmed in the CD31 immunofluorescence staining results shown in Figures S15C and S15D. On day 14, The relative CD31 expression levels of the TE-CM-4 (139 ± 6%) and TE-CM-4+NIR (164 ± 9%) were significantly higher than that of the control (89 ± 12%) and 3M (96 ± 19%) groups (Figure S15D). From the Masson trichrome staining images in Figure S14A, it can also be seen that the collagen fibers of the control group were irregularly distributed with slack structure, but the collagen fibers of the adhesive groups were more orderly arranged, and the collagen densities of the two adhesive groups were significantly higher ($p < 0.01$) than that of

the control and 3M groups, especially on the 14th day, the application of TE-CM-4+NIR induced the highest collagen deposition (Figure S14C). These results demonstrated that the administration of TE-CMBAs with/without NIR irradiation can significantly promote acute wound healing through the modulating the inflammatory microenvironment to inhibit the secretion of pro-inflammatory cytokines, and enhance angiogenesis during wound healing.

References

[1] X. Yuan, Y. Zhao, J. Li, X. Chen, Z. Lu, L. Li, J. Guo, *J. Mater. Chem. B* **2021**, *9*, 8202.

[2] X. Lu, S. Shi, H. Li, E. Gerhard, Z. Lu, X. Tan, W. Li, K.M. Rahn, D. Xie, G. Xu, F. Zou, X. Bai, J. Guo, J. Yang, *Biomaterials* **2020**, *232*, 119719.

[3] M. Mehdizadeh, H. Wen, D. Gyawali, L. Tang, J. Yang, *Biomaterials* **2012**, *33*, 7972.

[4] K. Wu, M. Fu, Y. Zhao, E. Gerhard, Y. Li, J. Yang, J. Guo, *Bioact. Mater.* **2023**, *20*, 93.

Table S1. Nomenclature of different tannin-europium coordination complex crosslinked citrate-based mussel-inspired bioadhesives (TE-CMBAs) and the volume ratios between iC-E-Ca^{2+} (33 wt%) solution and TEC (15 wt%) solution. These adhesives were all crosslinked at room temperature.

Sample	iC-E-Ca^{2+}	TE-CM-1	TE-CM-2	TE-CM-4	TE-CM-10
iC-E-Ca^{2+}	20	20	20	20	20
TEC	0	1	2	4	10

Table S2. Mechanical properties of different TE-CMBAs at dry and fully hydrated (swollen) states.

	Tensile strength (kPa)		Elongation at break (%)		Modulus (kPa)	
Sample	Dry	Swollen	Dry	Swollen	Dry	Swollen
TE-CM-1	445.5 ± 89.2	56.0 ± 16.9	1417.6 ± 299.2	1127.8 ± 182.9	648.4 ± 91.1	6.8 ± 4.9
TE-CM-2	479.3 ± 27.9	83.0 ± 10.4	1384.2 ± 194.1	1049.8 ± 146.3	689.9 ± 79.0	15.4 ± 5.4
TE-CM-4	518.0 ± 35.3	121.9 ± 9.3	1310.1 ± 119.1	786.7 ± 42.7	810.8 ± 32.4	22.1 ± 17.0
TE-CM-10	624.3 ± 52.2	146.8 ± 18.5	735.2 ± 140.6	579.4 ± 99.9	1397.3 ± 54.7	48.9 ± 13.0

Table S3. Comparision between diabetic db/db mice and C57BL/6mice.

Category	Gender	Age (weeks)	Weight	Blood glucose value (mmol/L)	Wound pH value
C57BL/6	♂	8	25 ± 5.0	6.5 ± 2.0	7.25 ± 0.25
db/db	♂	8	50 ± 5.0	29.0 ± 4.0	6.25 ± 0.25

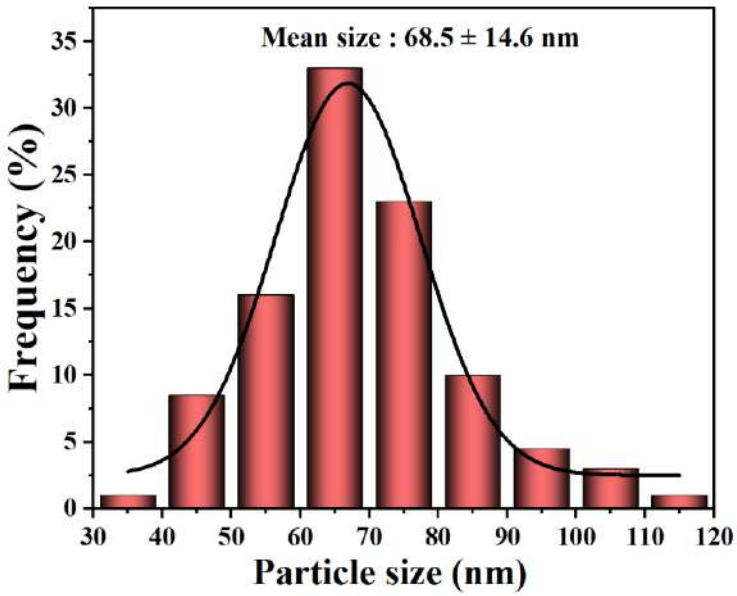

Figure S1. Particle size of TEC.

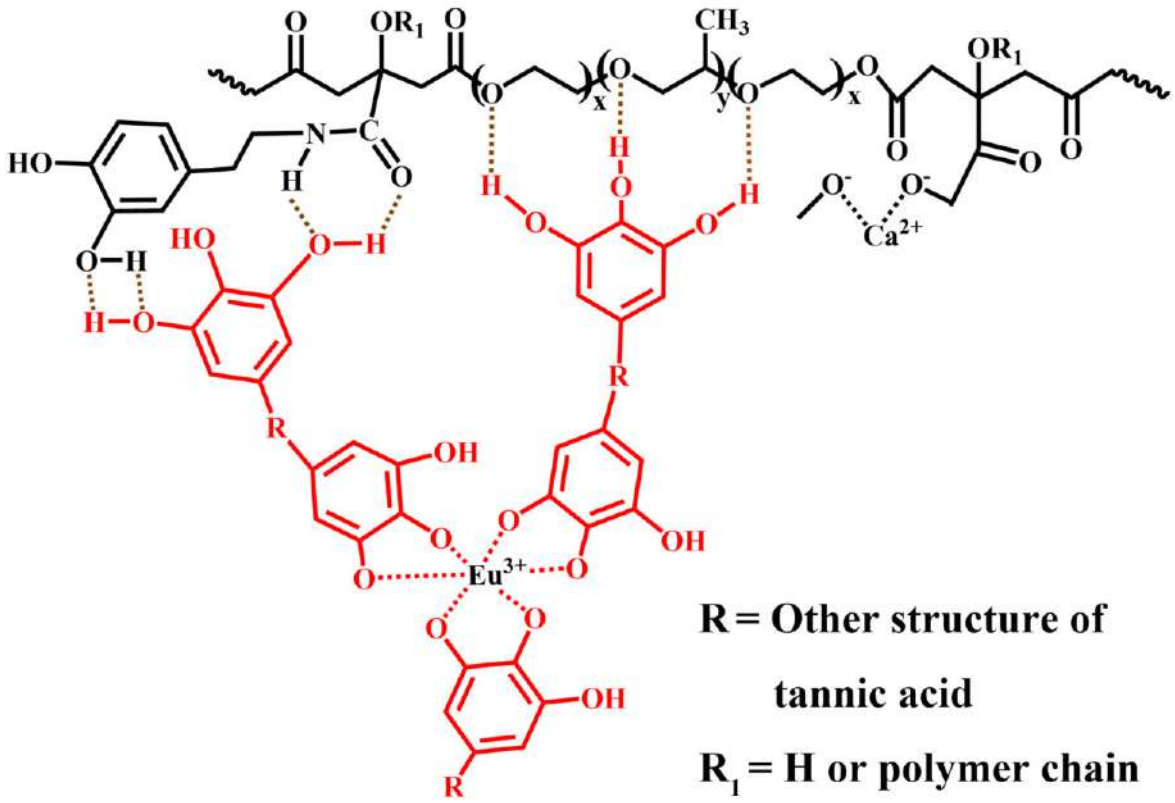

Figure S2. Structure diagram of the TE-CMBAs.

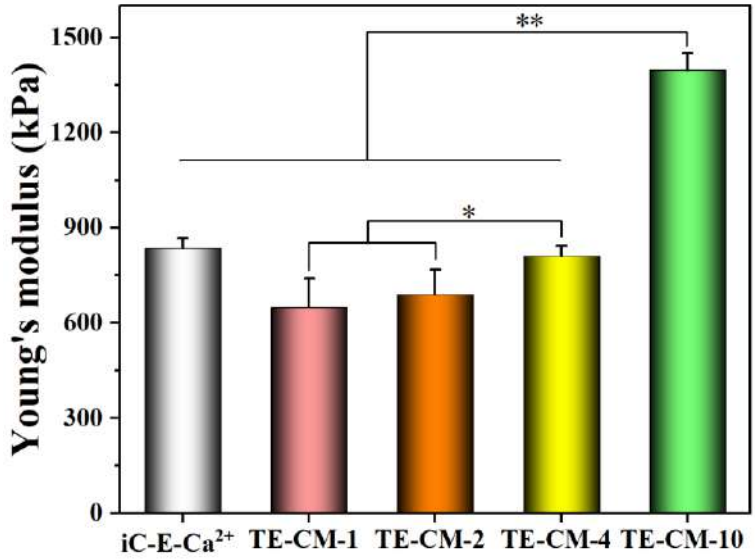

Figure S3. Young's moduli of different TE-CMBA formulations (n = 5). *$p < 0.05$, **$p < 0.01$).

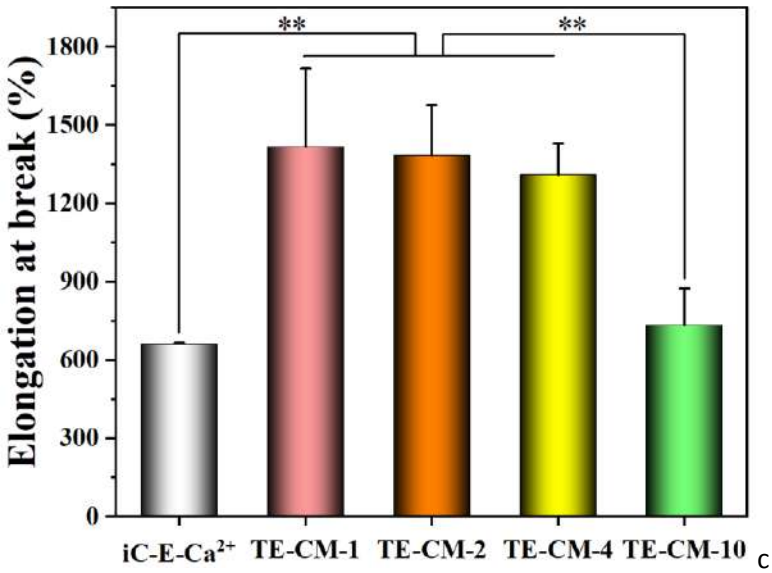

Figure S4. Elongations at break of different TE-CMBAs formulations (n = 5). *$p < 0.05$, **$p < 0.01$).

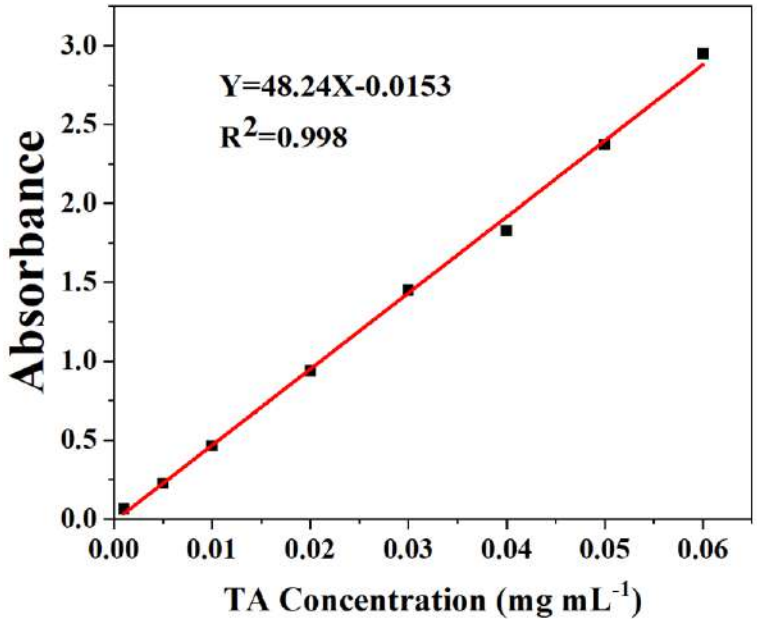

Figure S5. Standard curve of TA derived from UV-vis absorbance measurement.

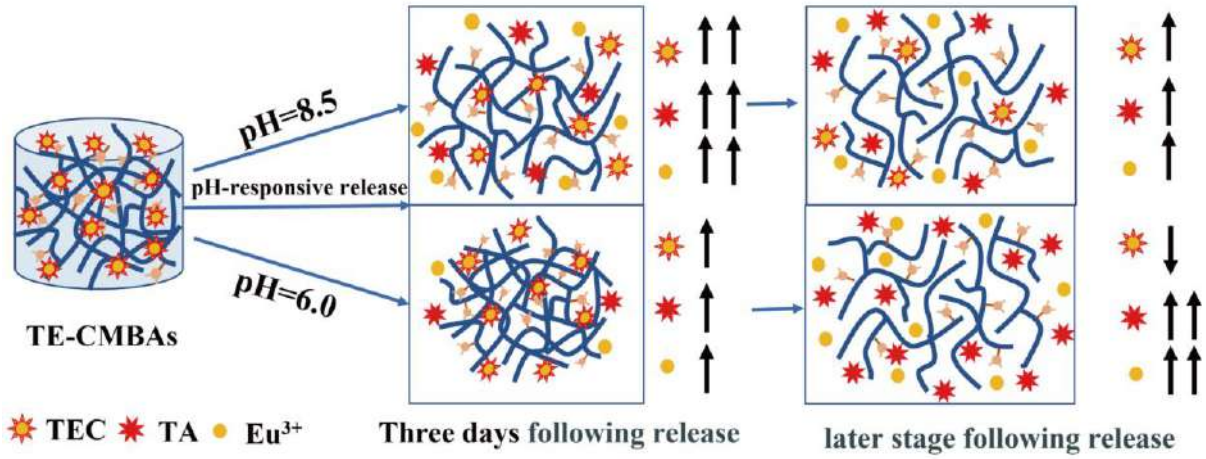

Figure S6. Illustration of pH-responsive Eu^{3+} & TA release mechanism from TE-CMBA.

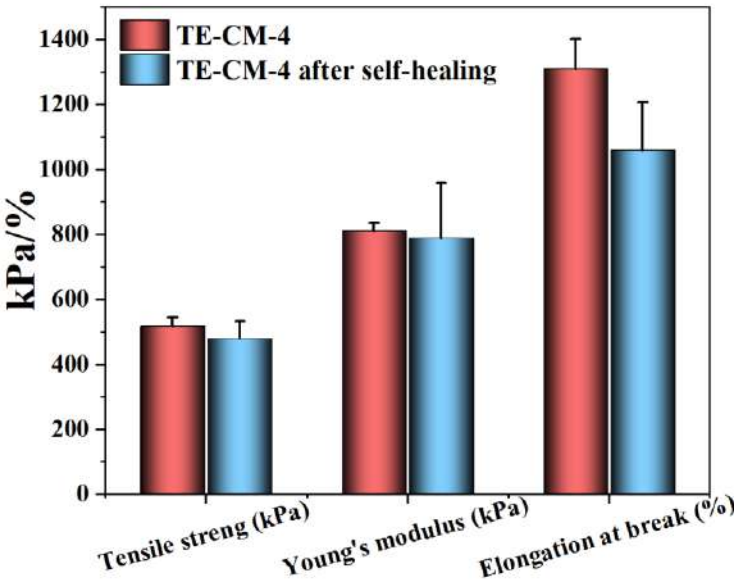

Figure S7. Mechanical properties of the hydrogel after macroscopic healing (n = 5).

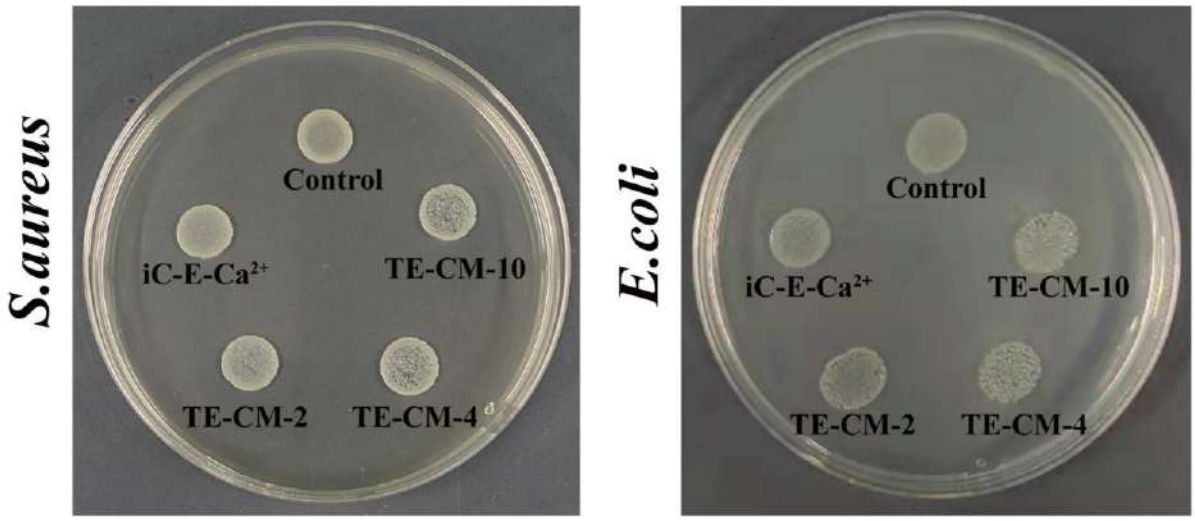

Figure S8. Contacting antibacterial activity of TE-CMBAs against *S. aureus and E. coli* without NIR irradiation.

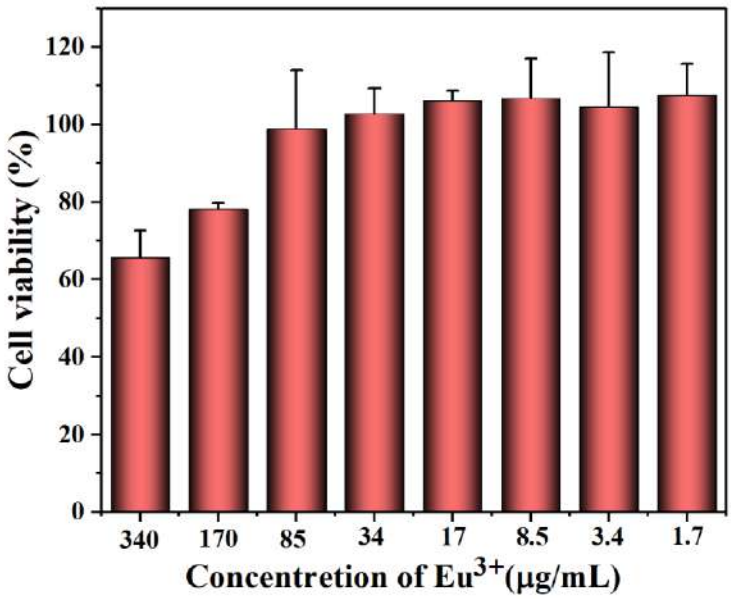

Figure S9. Cytocompatibility of Eu^{3+} (n = 4).

.

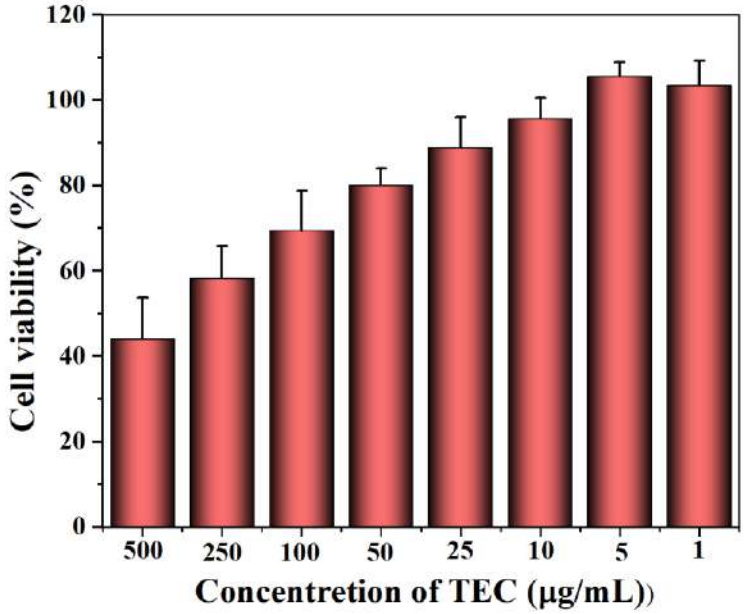

Figure S10. Cytocompatibility of TEC (n = 4).

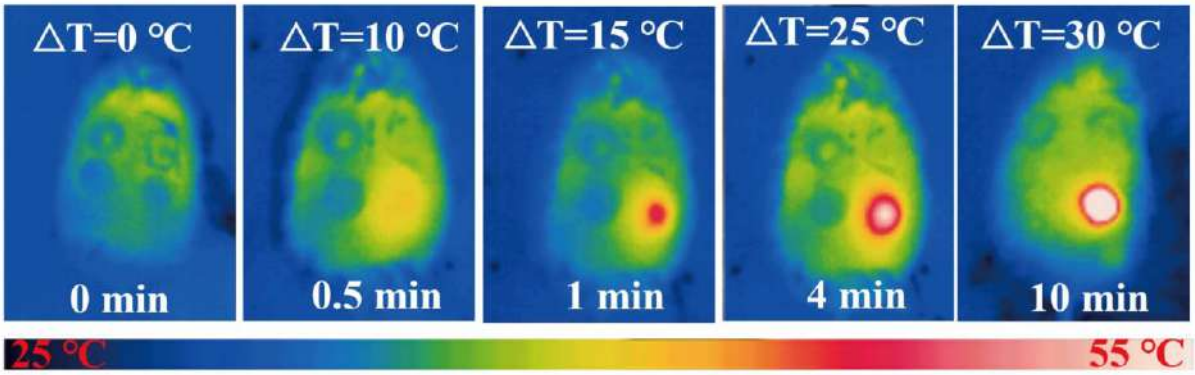

Figure S11. Thermographic images of TE-CM-4 on diabetic db/db mice upon NIR irradation.

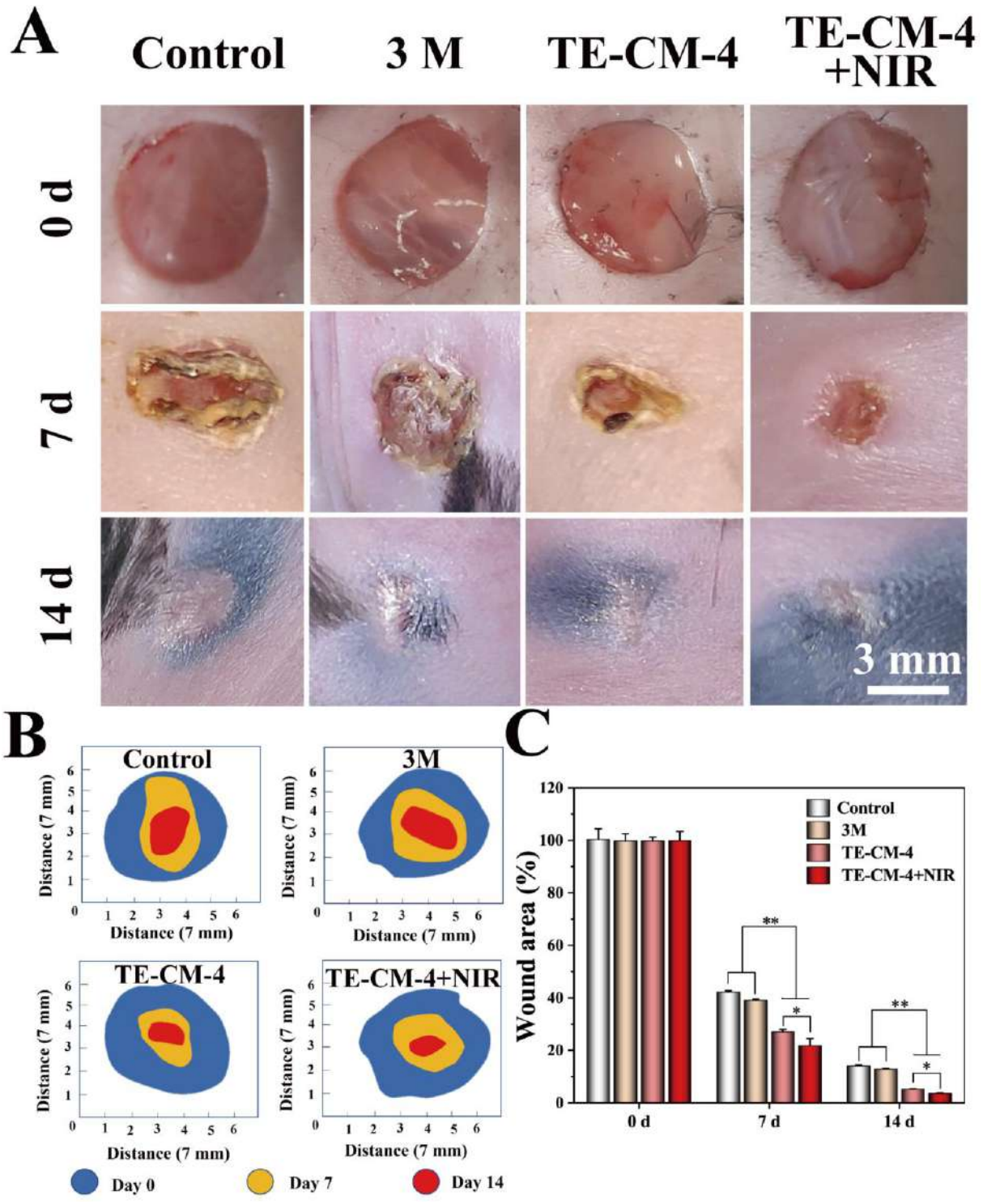

Figure S12. Wound closure performance of TE-CMBAs for acute wounds on C57BL/6 mice: (A) representative wound closure photographs; (B) schematic diagram of wound area change during 14 days; (C) the calculated relative wound areas on the 0, 7th and 14th day (n = 5). *p < 0.05, **p < 0.01).

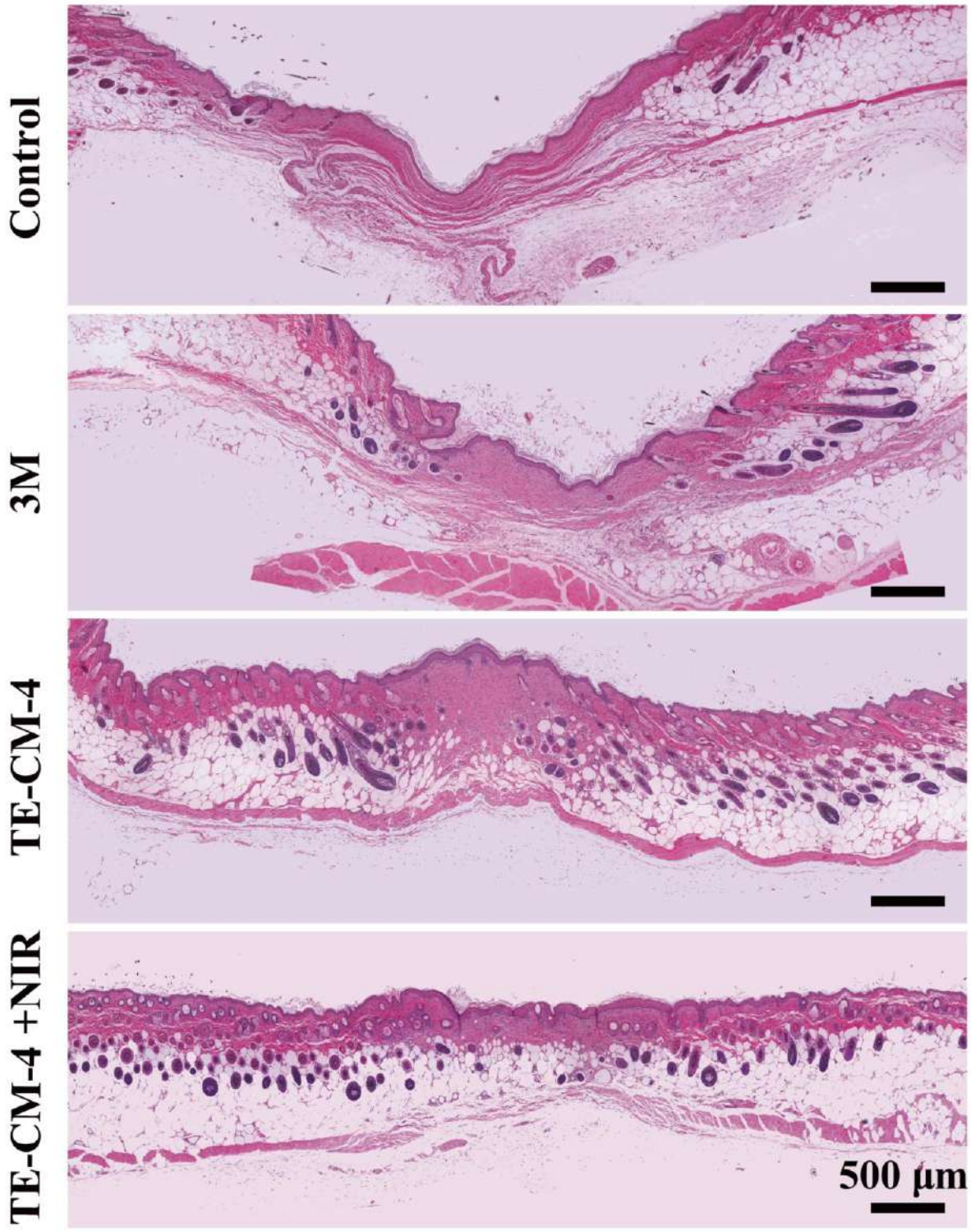

Figure S13. Wound closure performance of TE-CMBAs for diabetic wounds on db/db mice on day 21th.

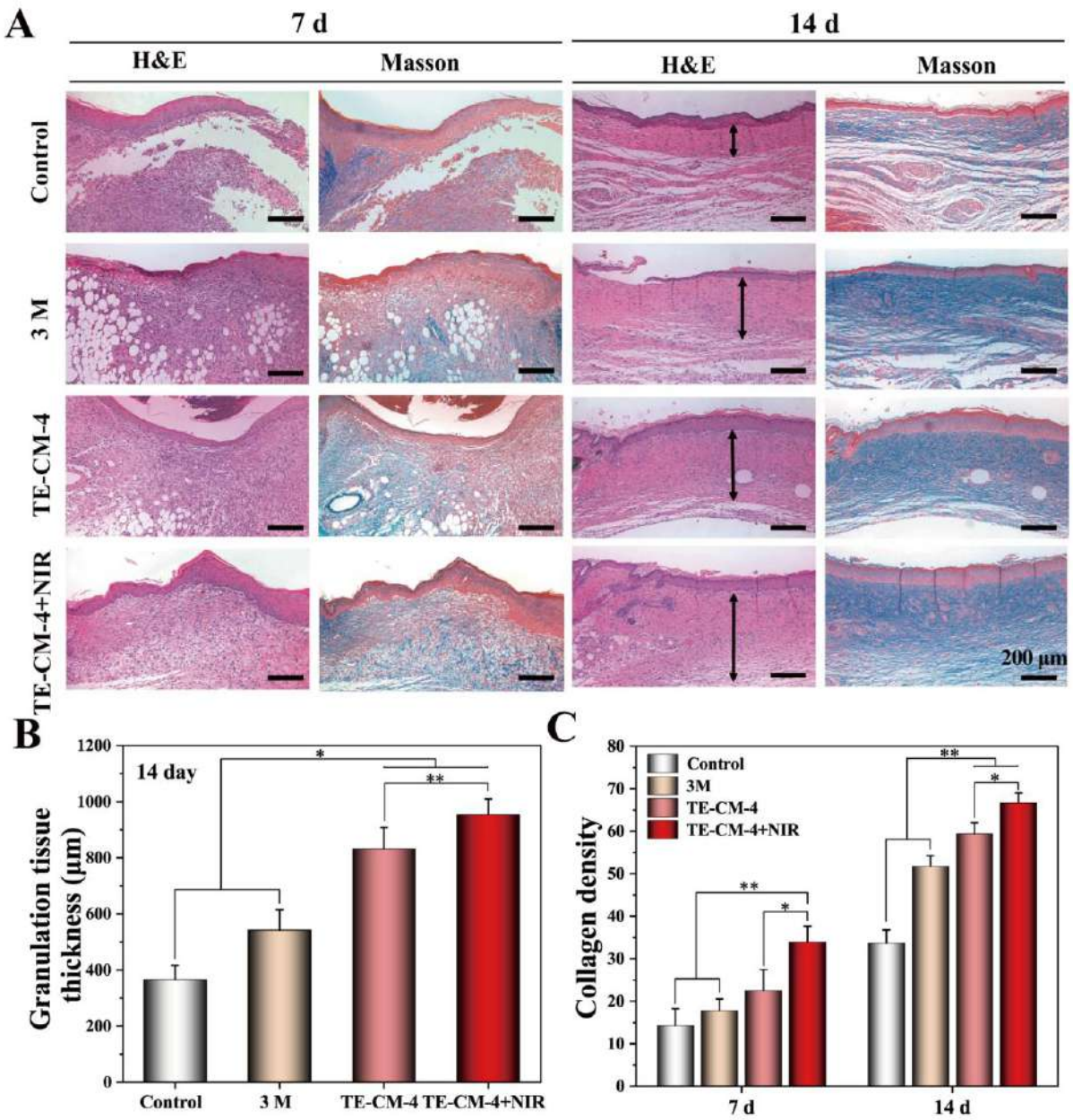

Figure S14. Histological staining results: (A) representative H & E and Masson trichrome staining images of the treated skin tissues on the 7th and 14th day post-surgery (Arrow: granulation tissue thickness); (B) quantitative data of granulation tissue thickness on the 14th day (n = 5); (C) quantification of collagen deposition and on the 7th and 14th day (n = 5). *p < 0.05, **p < 0.01.

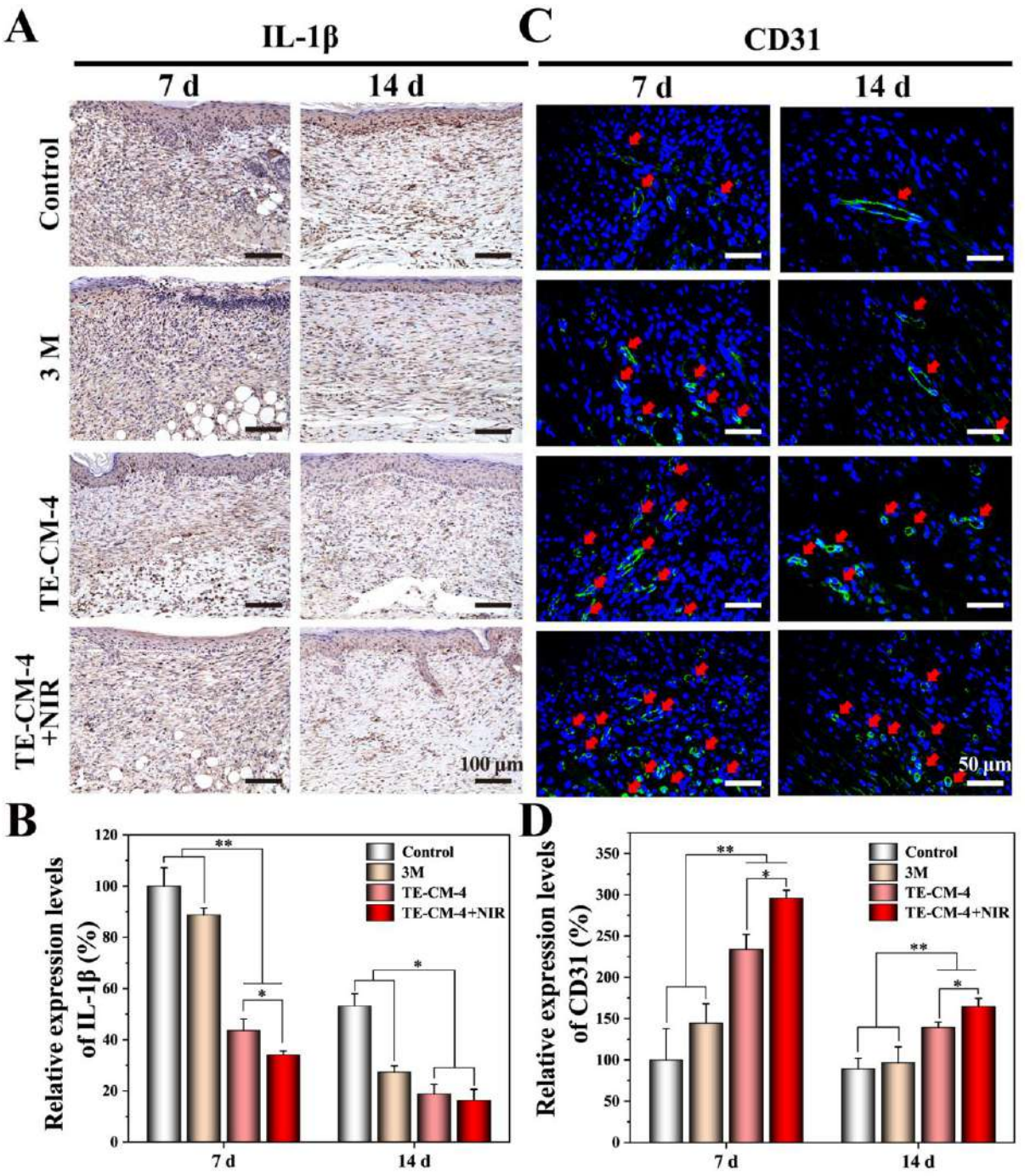

Figure S15. Immunohistochemical/immunofluorescence staining results of IL-1β and CD31: (A) representative IL-1β immunohistochemical staining images and (B) the quantified relative expression levels of IL-1β of different groups on the 7th and 14th day (n = 3); (C) representative CD31 immunofluorescence staining images and (D) the quantified relative CD31 expression levels of different groups on the 7th and 14th day (n = 3). For all data, the control group on day 7 was set as 100%, *$p < 0.05$, **$p < 0.01$.